THE RELATIONSHIP OF SOURCE PARAMETERS OF

OCEANIC TRANSFORM EARTHQUAKES

TO PLATE VELOCITY AND TRANSFORM LENGTH

by

NORMAN C. BURR

B.Sc., STATE UNIVERSITY OF NEW YORK, ALBANY

1975

SUBMITTED IN PARTIAL FULFILLMENT

OF THE REQUIREMENTS FOR THE

DEGREE OF MASTER OF SCIENCE

at the

MASSACHUSETTS INSTITUTE OF TECHNOLOGY

May, 1977

Signature of Author ....................................
Department of Earth and Planetary Sciences,
May 12, 1977

Certified by ...........................................
Thesis Supervisor

Accepted by ............................................
Chairman, Departmental Committee
on Graduate Students

## ABSTRACT

THE RELATIONSHIP OF SOURCE PARAMETERS OF

OCEANIC TRANSFORM EARTHQUAKES

TO PLATE VELOCITY AND TRANSFORM LENGTH

by

NORMAN C. BURR

Submitted to the
Department of Earth and Planetary Sciences
on May 12, 1977
in partial fulfillment of the requirements for the
degree of Master of Science

The source parameters of large earthquakes on oceanic transform faults are closely related to the thermal and mechanical properties of oceanic lithosphere. Several characteristics of these earthquakes (including magnitude, moment, apparent stress $\eta\bar{\sigma}$, and stress drop $\Delta\sigma$) are synthesized according to local plate velocity V, ridge-ridge offset L and average fault width W estimated by Brune's method. Several relationships result: (1) the maximum moment $M_o$ decreases with V; (2) $M_o$ increases with L for L < 400 km and may decrease for greater offsets; (3) $\eta\bar{\sigma}$ does not clearly depend on either V or L; (4) the maximum estimated W(V) decreases with V; (5) the minimum estimated W(L) increases with L; and (6) the largest earthquakes on long transforms occur near the transform center. Most of these relationships can be explained by thermal models for spreading centers if seismic failure occurs only at temperatures below a fixed value.

The inversion of slip rate and magnitude data by transform confirms this explanation and gives an estimate for the temperature of the boundary separating stick-slip and stable sliding. The actual thermal structure around oceanic transforms is not known but the idealized models used in the inversion give a temperature range, for the brittle to ductile boundary, of 75° to 125°C. Accounting for the possible uncertainties in the thermal structure, a temperature range of 50° to 300°C is proposed. This temperature range is consistent with laboratory investigations of slip in rocks of compositions that are representative candidates for the material being faulted in oceanic transforms.


Thesis Supervisor: Sean C. Solomon
Associate Professor of Geophysics

# TABLE OF CONTENTS

ACKNOWLEDGEMENTS

I would like to express my gratitude to my advisor, Sean Solomon, for suggesting the topic of this thesis and being constantly available for help with any and all problems. Randy Richardson, Bill Ellsworth, and George Zandt also provided valuable insight at various stages in my research. Special thanks go to Steve Taylor and Mike Fehler for the many stimulating conversations we had and for making life in the Green Building bearable. I must also thank Ellen Loiselle for her typing skills during a time of need.

This research was supported by the National Science Foundation under NSF Grant EAR75-14812 and by the Advanced Research Projects Agency and monitored by the Air Force Office of Scientific Research under contract F44620-75-C-0064.

## INTRODUCTION

Due to the spherical nature of the earth, the movement of one lithospheric plate with respect to another can be described as a rotation about an instantaneous pole of rotation. When this motion results in the two plates moving apart, a ridge and transform system will tend to form nearly along great circles, or lines of longitude, through the instantaneous pole and transforms tend to form along lines of latitude. Motion on these transforms is almost pure strike-slip on very high angle faults. This thesis is concerned with how transform length and slip rate affect the earthquakes produced on oceanic transforms and to what depth brittle failure occurs.

There are several terms which will be referred to frequently and these warrant some discussion. By transform, we mean that region between ridge crests which is undergoing active slip. Each transform is characterized by a length L, the distance between ridge crest segments, and a width W, the depth above which brittle failure occurs. This width may not be the same at all points along the transform but represents rather the average depth. As more detailed mapping is being done on the midoceanic ridge system, it is observed that transforms may range in length from 1000 km to less than 10 km. In this thesis only those transforms having earthquakes of magnitude 6.0 or above are studied. This eliminates most short transforms (under 80 km length).

The term fault will refer to the area of a single earthquake. It has a length $\ell$, which is not usually the transform length except in the case of very short transforms or very large earthquakes. The fault width w may correspond to the transform width.

The magnitude of an earthquake refers to the standard 20 second surface wave magnitude of Gutenberg and Richter (1942) or its equivalent. A more meaningful parameter than magnitude is the seismic moment of an earthquake (Aki, 1966), which can be related to fault area $\ell w$ and the average displacement $\bar{d}$ by

$$M_o = \mu \ell w \bar{d} \qquad (1)$$

where $\mu$ is the shear modulus.

Another useful term is moment sum $\Sigma M_o$, which is the sum of the moments for all earthquakes on a given transform within a specified time period. The moment sum can be related to the transform area A by

$$\Sigma M_o = \mu AVT \qquad (2)$$

(Brune, 1968), where V is the slip rate or full spreading velocity at the ridge, T is the time period over which the summation is taken, and A = LW. This equation assumes that all of the slip on the transform depth W is accomplished by brittle failure and that the sample time is long enough to get a representative quantity of earthquakes.

In the following sections these parameters will be compiled and related to each other and to thermal structure toward the end of better understanding the nature of seismic slip along oceanic transforms.

## DATA

Two largely geometrical properties of ridge-ridge transforms are length and slip rate. These two properties combined with the seismic source parameters of earthquakes occurring on each transform make up the data set used in this thesis.

Sixty oceanic transforms have been surveyed and documented in the literature well enough so that their location and length can be determined. The sources of these determinations are: Anderson et al. (1972); Bonatti and Honnorez (1976); Collette et al. (1974); Fisher et al. (1971); Forsyth (1975); Fox et al. (1976); Herron (1972); Klitgord et al. (1973); Mammerickx et al. (1975); Molnar et al. (1975); Norton (1976); Olivet et al. (1974); Sclater et al. (1976); Sykes (1967); Thompson and Melson (1972); van Andel et al. (1973); Vogt and Johnson(1975); and Weissel and Hazes (1972). This list accounts for most of the large midoceanic transforms except for two notable exceptions: the Africa-Antarctic plate boundary and the complicated zones on the East Pacific Rise near 20° south and 34° south. Inadequate mapping in these areas is the cause of their exclusion from this study. The error in measurement of the transform length is variable but is generally less than 15%. The spreading rate for each transform is calculated using the poles and angular velocities of Minster et al. (1974).

The most commonly used earthquake source parameter is magnitude. All of the reported earthquakes on each transform since the early 1900's with magnitude 6.0 or greater are compiled in Appendix 1 (and in condensed form in Table I) by fracture zones. Events with magnitudes less than 6.0 are usually not reliably reported, or located, especially in the early 1900's. The earthquake catalog and magnitude scale used for earthquakes between 1920 and 1952 are from Gutenberg and Richter (1954); for the years 1953 to 1965, Rothe (1969) is used; and for the events from 1966 to 1975, the 20 second surface wave magnitudes from the C.G.S./N.O.A.A./U.S.G.S. are taken (except for those events noted in Table II). Geller and Kanamori (1977) have shown that the calculation used in present day determinations of the 20 second surface wave magnitude is close to that used by Gutenberg and Richter. The assumption is made that the magnitudes from Rothe (1969) are also on an equivalent scale.

Only for the recent earthquakes (1963 and later) have other seismic source parameters been measured by spectral analysis. These parameters are seismic moment $M_o$, apparent stress $\eta\bar{\sigma}$, and stress drop $\Delta\sigma$. The apparent stress is the product of the average shear stress $\bar{\sigma}$ on the fault before and after faulting and an unknown efficiency factor $\eta$. Stress drop is the difference between the initial and final shear stress on the fault. Several researchers have looked at earthquakes occurring on transforms and analyzed the amplitude spectra of the surface waves produced. The results of these studies are compiled in Table II.

Apparent stress has been calculated for each event using the equation:

$$\eta\bar{\sigma} = \mu E/M_o \qquad \text{(Aki, 1966)} \qquad (3)$$

where $\mu$ is the shear modulus ($3.3 \times 10^{11}$) and E is the seismic energy:

$$E = 5.8 + 2.4\ m_b \qquad (4)$$

and

$$E = 11.8 + 1.5\ M_s. \qquad (5)$$

$M_s$ and $m_b$ are the surface and body wave magnitudes, respectively. Note that the energy equation using $M_s$ is valid only for surface wave magnitudes 6.5 and greater. Apparent stress has been compiled for $m_b$ (ISC) and $M_s$ in Table II.

Stress drops have been reported in the literature for several transform events. Stress drops for two earthquakes on the Gibbs fracture zone analyzed by Kanamori and Stewart (1976) can be calculated using

$$\Delta\sigma = \frac{2M_o}{\pi \ell w^2} \quad \text{(Knopoff, 1958)} \quad (6)$$

Kanamori and Stewart (1976) calculated a length from waveform analysis of body waves. Using a fault width of 5 to 10 kilometers, the possible range of stress drops for both earthquakes is between 30 and 140 bars.

Udias (1971) calculated $\Delta\sigma$ using the directivity function for surface waves; he found stress drops in the 10 to 20 bar range for 2 earthquakes. An attempt was made to determine fault lengths for the rest of the published moments, using relocated aftershock data, but only the 1974 event already studied by Kanamori and Stewart (1976) had more than two aftershocks.

The seismic moments for six additional transform earthquakes have been calculated for this study (Table II). The method used, described in Richardson and Solomon (1977), consists of computing the amplitude spectra of horizontally polarized shear waves and then correcting for the effects of instrument and travel path, thus obtaining the source spectrum. The moment is computed from the long period spectral amplitude level ($\Omega_o$) by:

$$M_o = \frac{4\pi\rho\beta^3}{RG}\Omega_o \quad \text{(Keilis-Borok, 1960)} \quad (7)$$

where $\rho$ and $\beta$ are density and shear wave velocity, respectively, at the source, R is a correction for radiation pattern, and G is a correction for geometrical spreading, attenuation, and the free surface. Fault plane solutions for the South Pacific events come from Molnar et al. (1975) and those for the southwest Indian ridge events are from Norton (1976). Four to seven stations, away from SH modal planes, were selected for each event and the moment calculated. The mean value for each event is reported in Table II and the value for each station is displayed in Table III. The geometric mean of the amplitude spectra for each event, corrected as in equation (7), is displayed in Appendix 2.

A method for estimating fault length without using aftershocks is achieved by finding the corner frequency ($f_o$) of the amplitude spectrum:

$$\ell = .20\beta/f_o \qquad \text{(Madariaga, 1977)} \qquad (8)$$

where $\beta$ is the shear wave velocity (3.9 km/sec). The corner frequency is a difficult parameter to read and on the spectra studied only a range of possible values can be determined. This range is between .02 and .05 Hz and seems to be comparable for all six events. The corresponding fault lengths are 15 to 40 km thus giving stress drops between 1 and 60 bars. It is not obvious, but stress drop may increase with moment.

Norton (1976) noted a gap in seismicity for the period 1900 to present near 49°S, 32°E on the southwest Indian ridge. This gap corresponds to the location of a magnitude 7.9 event (Gutenberg and Richter, 1954) on 10 November 1942, for which Brune and King (1967) have calculated a moment. Norton suggested that this also marks the approximate location of a fracture zone that may be 400 km long. This event and its transform have been included in both Tables I and II. Another event of magnitude 7.7 occurred nine years later on the same ridge, 3000 km away at 34°S, 57°E. The moment for this event has not been calculated and the geometry of its associated transform is not defined, so it has not been included.

## RELATIONS CONCERNING SOURCE PARAMETERS, TRANSFORM LENGTH, AND SLIP RATE

It has already been shown that the seismic moment is directly related to the product of fault area and displacement, and that the summation of moments is related to the product of transform length, width, slip rate, and sample time. To gain insight into the vertical structure of transforms using these relations, one can use the earthquakes for which a moment can be measured directly. But this only accounts for the last few years, since it has only been recently that good seismograms have been readily available. Thus it would be informative if seismic moments could be obtained from the magnitudes which have been compiled in Appendix 1, thereby quadrupling the sample time. To do this we will look at the graph of moment vs. magnitude which displays those events for which a moment has been calculated directly from a seismogram.

Figure 1 shows the earthquakes with a measured moment and a surface wave magnitude reported by the U.S.G.S, the two events with $M_o$ and $M_s$ measured by Udias (1971) and the magnitude 7.9 event. The $M_o$ vs. $M_s$ curve from the $\omega^2$ and $\omega^3$ models of Aki (1967), as plotted by Brune and King (1967), are shown with dotted lines. The symbols represent the plate boundary where the earthquake is located (Table IV). It should be noted that the $M_s$ 6.5

event with a large moment has been documented by Kanamori and Stewart (1976) as being an unusual event. This event seems to have a hole in the spectrum at 20 seconds (Solomon, personal communication) so $M_s$ may underestimate the surface wave excitation.

Figure 2 is the $M_o$ vs. $M_s$ curve utilizing the data in Figure 1 plus the magnitudes calculated by Rothe (1969). Considerable scatter results, but in a least-squares sense the data still fit the previous figure quite well. For the rest of this thesis the data of Figure 1 will be used as a basis for comparison with other moment magnitude curves to be calculated.

There is some debate at present whether the $\omega^2$ source model is correct (Geller, 1976) but for lack of a better choice, and since it seems to fit the data fairly well, the $\omega^2$ curve will be used to translate $M_s$ (or M) into $M_o$ for future plots.

The graph of $M_o$ vs. spreading velocity (V) is shown in Figures 3 and 4 where $M_o$ is either measured or estimated from the magnitude, respectively. Figure 5 is the moment sum vs. slip rate. All three graphs show an upper bound, or maximum, moment which decreases as spreading rate increases.

The next three figures (6,7,8) show the relation of $M_o$ and $\Sigma M_o$ vs. transform length. The most obvious observation on all three graphs is that the upper bound on $M_o$ and $\Sigma M_o$ increases as the transform length increases for

for lengths less than 400 km. Above 400 km length there is an apparent decrease of maximum moment with increasing length. Since the magnitude 7.9 event may represent the moment needed to break the entire transform it may be mechanically unrealistic to break a substantially longer fracture zone (e.g., Romanche, 950 km long) so the bound on moment may actually decrease after 400 km length. In Figure 6 there are two events with large moments on 130 km transforms. Their moments (from Wyss, 1970) may be overestimated or they, too, may represent breakage of the entire transform. This is especially true of the 7.0 event on the Tjorn fracture zone. Notice, as with Figures 3-5, that the magnitude 7.9 event contributes to and accentuates the trend but does not of itself produce it.

Another trend apparent on the $M_o$ vs. L plot is for the minimum $\Sigma M_o$ to increase as transform length increases. This trend and the above two trends indicate that both slip rate and length are affecting faulting on these oceanic transforms. To put these two effects together one can solve for average width in Brune's (1968) formula:

$$W = \Sigma M_o / \mu LVT \qquad (9)$$

Finding a value for T (sample time) is complicated because transforms may be inactive for substantial periods of time and because some earthquakes above magnitude 6.0 have not been reported. The value of fifty years seems to allow for both problems on most transforms but there may be an error as large as ±15 years for some. $\mu$ is taken to be $3.3 \times 10^{11}$ dynes. An average width has been calculated for each transform by this method and compiled in Table I. The two major assumptions to keep in mind for the above formula are that (1) all movement on the fault is brittle failure, and (2) due to the logarithmic nature of the $M_o$ vs. $M_s$ curve, earthquakes smaller than $M_s = 6.0$ will not have a substantial effect on the moment sum. Taking these errors into consideration W is probably good to a factor of 1.5 or, at worst, a factor of 3.

Figure 9 shows a plot of W vs. transform length. The dotted lines approximate the trend of transforms having approximately the same slip rate. There is a trend for width to increase as transform length increases for transforms of similar velocity.

To explain this observation it is necessary to look at what is occurring along the transform. At the ridge crest hot material is added to one side of the transform, and as this material moves away from the ridge crest it cools and contracts. Rocks at high temperature will tend to flow and not fracture so one would expect that right near the ridge crest, where the crust is very hot, brittle failure may only occur very near the surface. As the crust cools and moves away from the ridge, brittle failure will occur deeper in the crust.

Consider the fact that along faster transforms the isotherms in the crust are closer to the surface than along slower ones, also notice in Figure 9 that the slower transforms get wider more quickly as length increases. From these two observations, one can postulate that the area of brittle failure is controlled by the depth to a certain isotherm. It is this idea that will be further explored in the next section.

The next graph (Figure 10) shows a large decrease in computed width as spreading rate increases. For clarity, the graph only shows widths less than 8 km. There are some larger widths corresponding to velocities less than 3.0 cm/year. This graph can be partially explained by the above discussion of width vs. length but another factor causing this relation is shown in Figure 11.

Figure 11 is a plot of transform length vs. spreading rate and it shows the maximum lengths decreasing as spreading rate increases. The cause of Figure 11 could involve many diverse factors. First of all, the pattern may be merely a coincidence that will change with time. Such a 'coincidence' as this must have held, however, for the last 100 m.y. because the 950 km-long Romanche fracture zone has been in existence that long and the Mid-Atlantic ridge has had about the same spreading rate relative to other ridges as it does now. In fact, most of the major transforms can be traced back to continental margin offsets via fracture zones. Thus it is the original pattern by which continents break apart that determines where many of the large transforms will occur.

Note that the East Pacific rise has mainly small fracture zones. This could be due to the fact that this ridge has not represented the junction between two continents for the last few hundred million years, if ever.

One thing that would tend to break up a transform is a change in the location of its pole of rotation. This would put the transform under either compression or extension. Extension would form a spreading center within the transform and compression would shorten or deform the transform and might lead to ridge jumps or asymmetric spreading. In the right circumstances asymmetric spreading, or a ridge jump, could also lengthen a transform. All of the above effects would be felt most heavily on a transform with a fast slip rate due to its hotter, weaker crust. It is possible that the least energy configuration of a ridge would be many small transforms as opposed to a few large ones, but that point is debatable. Perhaps long fracture zones inhibit changes in spreading poles by their inability to change shape and restrict spreading rate by frictional resistance.

Apparent stress was plotted against all the other parameters but no one clear relation could be discerned. Thus, from the available data, it does not appear that spreading rate or transform length have a noticable affect on the stress field around oceanic transforms.

Figures 12 and 13 are graphs of $m_b$ (U.S.C.G.S.) and $m_b$ (I.S.C.) vs. $M_s$, respectively. This ratio of $m_b$ to $M_s$ is quite unique for oceanic transforms, that is, $M_s$ is almost always higher, sometimes by as much as 1.2 units. Dip slip earthquakes and continental strike-slip earthquakes yield a higher $m_b$ to $M_s$ ratio. In fact, Shakal (1975) reports that it is possible to discriminate between dip slip and strike-slip earthquakes along the Mid-Atlantic ridge with fairly reasonable accuracy using this method. There are basically two reasons for this difference. First, strike-slip mechanisms are more efficient at generating surface waves than dip slip events and second, for events near oceanic ridges, the body waves are attenuated relative to surface waves. This type of attenuation does not affect continental strike-slip events. Oceanic earthquakes may also generate larger 20 sec surface waves than continental events of comparable $m_b$ because of generally shallower focal depth (Tsai, 1969; Tsai and Aki, 1970).

THE INVERSE PROBLEM

In the previous section a moment-magnitude relation was used to assign moments to earthquakes so that information about the fault width could be ascertained. If this is considered the forward problem, then the inverse problem would be to assume something about the width and then invert the earthquake data to get a moment-magnitude curve. The depth to a certain isotherm within a transform, as suggested in the last section, is assumed to be the parameter that will properly relate length and slip rate.

Ideally what we need is the thermal structure of each oceanic transform. To our knowledge, this has never been modeled and, until the geology and the factors controlling the topographic features within the slip zone are known, it will be difficult to determine. The thermal structure of normal oceanic crust, however, is reasonably well understood (e.g., Sleep, 1975). It will be assumed that such structure holds for each side of a transform as well. According to such spreading plate thermal models, a given isotherm is closer to the surface on the side of the fault closest to the spreading center. It is only in the center where a given isotherm is at the same depth on both sides of the fault. If a single isotherm limits brittle behavior, then there are two possible bounds on the shape of the faulting area, as shown in Figure 14. The first area represents the shallowest depth of a given isotherm and the second represents the greatest depth to a given isotherm.

To pose the inverse problem we first write the equation for the predicted moment sum $D_i$ for the $i^{th}$ transform from the fault-slip theory of Brune (1968):

$$D_i = \mu S_i V_i T_i \tag{10}$$

where D,V, and T are the transform area, slip rate, and sample time, respectively. Using the areas from the discussion (Figure 14a or b) D can be calculated once an isotherm is specified. Utilizing the earthquakes on the $i^{th}$ transform, the moment sum $M_o$ from seismic observations is

$$\Sigma M_o = \sum_{j=1}^{13} A_{ij} C_j \tag{11}$$

where $A_{ij}$ is the number of earthquakes of the $j^{th}$ magnitude on the $i^{th}$ transform, and $C_j$ is the moment corresponding to the $j^{th}$ magnitude, according to the moment-magnitude relation to be determined. Note that in this study only the thirteen discrete magnitudes 6.0, 6.1, 6.2, ..., 7.2 are used. The three transforms with events larger than 7.2 are not included because too few events of such magnitude have occured to perform meaningful inversion. The A matrix is compiled in Table I.

Equating the right-hand sides of (10) and (11) and solving for the C's will give a moment-magnitude relation that can be compared, for each adopted isotherm, to the data shown in Figure 1. If the trends are the same it will confirm the hypothesis that the depth to a certain isotherm is the parameter that appropriately combines slip rate and transform length to control fault area. The position of the resultant curve will be determined by the limiting temperature picked to calculate the fault areas. Thus matching the position of the curve to the data in Figure 1 will give some idea as to what temperature is controlling the depth of brittle failure.

The combination of the two equations above result in the matrix equation:

$$D = AC \tag{12}$$

which is an overdetermined set of linear equations. Premultiplying equation (12) by $A^T$ (the transpose of A) results in a system of linear equations,

$$A^T D = A^T AC \tag{13}$$

where $A^T A$ is a square, nonsingular, symmetric matrix. The solution vector C can be found using standard routines for solving a system of linear equations.

Since the relation log moment vs. magnitude can be approximated by a straight line, at least for magnitudes less than about 7.0, it is convenient to do a linear least squares fit of the log of the vector C as a function of the respective magnitudes. This gives a slope and a position to a line which is easily compared to other log moment-magntidue relations. The discrete solution (C) is important, in some respects, because it indicates how well the moment for each magnitude is determined. However, in other respects, the discrete solution is not as important as the least-squares solution because the earlier magnitudes (Gutenberg and Richter, 1954) are typically given only to the nearest quarter, rather than tenth, of a magnitude unit.

Figure 15 shows the results of the inversion of 57 transforms using four different temperatures to determine the fault area (Figure 14a). The three transforms in Table I with earthquakes of magnitude greater than 7.2 have not been used (Vema, transforms at 7°N, 36°W and 49°S, 32°E). When the least-square lines are compared with the data from Figure 1, it is evident that the isotherm that will best match the moment-magntude data is about 150°C.

The discrete solution (Figure 16) for the above 57 transforms shows that each moment is not very well defined and that they have only a trend of getting larger. Looking at the data there are several transforms which seem to have either an abnormally large or small number of earthquakes for their length and velocity. This is reflected in the width calculation in the previous section by inconsistent widths. These transforms are (from Table I):

1-2; 2-1; 3-1; 3-2; 7-1; 10-6; 12-1; and 14-3 where the first number represents the plate boundary (Table IV) and the second indicates the particular transform on that plate boundary.

The discrete solution for the remaining 49 transforms (Figure 17) has a much more consistent determination of moment and in the least-squares sense (Figure 18) the slopes remain the same as the previous solution (Figure 15), but the position of each line is moved up slightly. Using the 100°C isotherm, which is the best fit for this case, an average width has been computed by dividing the area above the isotherm for each transform by the transform length. These widths have been compiled in Table I. The eleven anomalous transforms may have a nonrepresentative sample of earthquakes or may be affected by some other phenomenon more severely than for the others.

The slope of the lines in Figures 15 and 18 are very close to the $\omega^3$ plot. This could indicate that the model is correctly giving the moment-magnitude relation. However, the data from this study and the one by Brune and King indicate that the moment-magnitude relation is best described by a curve intermediate between the $\omega^2$ and $\omega^3$ models. This discrepancy could be due to the least-squares solution smoothing out any trend for a slope increase at higher magnitudes, but one would still expect a slope slightly larger than that of the $\omega^3$ curve. The discrepancy could also be caused by the fault width of higher magnitude earthquakes being determined by a higher temperature than lower magnitude events. This would partially explain some of the anomalous widths obtained for the Vema, Tjorn, and other transforms with large magnitude events for their offset lengths.

One model for the loading and rupture of a transform fault (Thatcher, 1975) is based on the hypothesis that loading occurs along the base of the fault by aseismic creep of the underlying material. This model would suggest that the fault depth is limited by the ability of material to creep far enough to precipitate the seismic slip . It is possible that for larger magnitude events a large amount of creep is needed, and that only that material at a higher temperature can creep the required distance. This may be in contrast to lower magnitude events, which require only a small amount of creep that can be accomplished by shallower, lower temperature material.

There are several other factors which could affect the positioning of the predicted curves in Figures 15-18. The first is the addition of earthquakes less than magnitude 6.0. This will produce a downward shift, so that a higher temperature will produce the best fit. The fact that moment-magnitude relations are logarithmic indicates this effect is small; that is, the moments for smaller magnitudes do not make a substantial contribution to the moment sum. Another uncertainty is the earthquake sample time for each transform. The sample time for Figures 15 to 19 has been taken to be fifty years. When other reasonable sample times are taken, both constant and variable, the lines shift slightly. Taking these uncertainties into account, the isotherm that fits can be specified only to lie between 100°C and 175°C.

The actual method of slip on a transform may introduce two additional uncertainties. The time period over which earthquakes have been catalogued may not be long enough to get a good representation of activity. Further, if shear stresses are relieved by aseismic slip, such as along the central San Andreas (Savage and Burford, 1971), then determining the slip by any seismic method will underestimate the actual movement. There is no data on how much this latter possibility will affect the results.

The largest change in position of the lines is produced when a larger area, such as that in Figure 14b, is used. Contrary to the previous variations, use of this definition of area results in moving all curves upward, thus decreasing the temperature of the isotherm that best fits the data (Figure 19).

This raises again the problem of what the thermal structure of a transform zone actually looks like. It is likely that Figures 14a and 14b based on the least or greatest temperature on one side of an idealized insulating fault, represent bounds on the true isotherm configuration. To determine the actual shape one must consider several factors: conduction of heat across the fault will tend to average the temperature on either side; at the ridge crests there is probably enough heat flow from the instru- sion of magma to keep the faulting very shallow; and at any distance from the ridge, the heat sink on the cold side of the fault will increase the depth of faulting rapidly. It is observed that most transforms are marked by a linear trough, from several hundred meters to several kilometers below the normal ocean crust, striking parellel to the transform axis. This topography will complicate the thermal structure; in particular, the values of the isotherms in the models (Figures 14a and b) may be too low for the shallow portions of the transform. Thus any estimate of the temperature controlling the transform width, using these models, would also be low. Three other factors affecting isotherm depth are the production of heat when brittle failure occurs, hydrothermal circulation in the highly sheared fault zone, and a composition difference between the transform zone and normal ocean crust necessitating a change in the conduction constant used in the thermal model calculation.

The inversion of the magnitude data does not resolve the actual shape of the isotherm, but only the specific isotherm that best fits the data given a general shape. That is, a 75°C isotherm and the area in Figure 14b fit the data just as well (Figure 19) as a 150°C isotherm and the area of Figure 14a (Figure 15).

One observation that resolves part of this problem of shape concerns the location on the transforms where large earthquakes occur. The locations of the earthquakes are not always precise enough to determine exactly where, in relation to the ridge crests, they occur, but in general larger earthquakes are located towards the centers of the transforms. A good illustration of this observation is the map in Figure 20 of the Romanche fracture zone. No earthquakes of magnitude 6.2 or greater occur closer than 60 km from the ridge crest, yet as noted earlier, earthquakes in the magnitude range 6.5 to 6.9 have typical fault lengths of 15 to 80 km. Thus the major reason for the central location of large magnitude events is the increase in fault width away from the ridge crests which allows larger magnitude events to occur. It is not due to large events rupturing a distance all the way to the ridge crest except in rare instances of very large events.

Trying to average over all transforms may not be ideal because of the different geometries controlling the interaction of the plates on either side of the transform. Some transforms may be under compression or extension if the poles of rotation for the individual plates are changing, or have changed. Another possibility, if the pole has remained fixed for a long period of time, is that the transform may be under slight extension from the cooling of the lithosphere on either side. If extension is the case, there may be some instrusion of mantle magma into the fracture zone thus raising the isotherm. Extension may be occurring in the North Atlantic (Collette *et al.*, 1974) but the fault widths seem to increase in these areas, rather than decrease, so the intrusion may have another effect. Transforms under compression and those changing shape to accomodate pole changes may be more susceptible to a stick-slip mechanism.

So far in this study we have shown that the inversion of slip-rate and magnitude data gives a consistent moment-magnitude relation, that is, if an isotherm limits the deepest extent of seismic failure. We have also seen that there are many uncertainties involved in the determination of the detailed thermal structure. Given all the uncertainties a conservative estimate for the temperature below which brittle failure occurs in oceanic transforms is in the range of 50° to 300°C.

The next question to be considered is: are these temperatures reasonable? Several investigators (Brace and Byerlee, 1970; Stesky, 1975) have looked at the boundary between stick-slip and stable sliding in natural rock samples. They have concluded that this boundary is dependent on temperature, pressure, and composition of the faulting material. At 4 kilobars pressure Stesky (1975) found that San Marcos gabbro and Twin Sisters dunite started stable sliding between 150°C and 200°C and that Mt. Albert peridotite started stable sliding well below 100°C. Thus the temperatures from the inversion correspond to those obtained in laboratory investigations on rocks which are representative candidates for the material being faulted in the transform.

## CONCLUSIONS

In this study of earthquakes occurring on oceanic transforms we have noted the following relationships. (1) Maximum moment, average fault width, and maximum moment sum all decrease with increased slip rate. (2) Maximum moment and maximum moment sum increase with transform length up to 400 km length and may either decrease or continue to increase with length for longer transforms. (3) Minimum moment sum and average width also increase with transform length. (4) Larger earthquakes generally occur towards the center of a transform. From these observations it was hypothesized that an isotherm in the transform zone controls the lower limit of the area over which brittle failure occurs. The inversion of magnitude data shows this statement is reasonable and gives a range of isotherms that could be controlling faulting of between 75°C and 175°C. Uncertainties in the shape and depth of the isotherms within the transform widen this range to between 50°C and 300°C. This range is consistent with laboratory studies on the temperature of the transition from strike-slip to stable sliding for rocks of similar composition to those thought to be in the transform zone.

Further study is needed to constrain the thermal structure of the transform so that a more accurate determination of temperature controlling the fault width can be defined. The moment magnitude curve needs more data for higher magnitudes so that a discrimination can be made between $\omega^2$ and $\omega^3$ models. From this it may be possible to determine whether or not higher temperatures are controlling the fault width for earthquakes having a large moment. The analysis of more source spectra could lead to a determination of relations between stress drop, apparent stress, slip rate, and transform length which have so far been undefined.

REFERENCES

Aki, K., Generation and propagation of G waves from the Niigata earthquake of June 16, 1964. Part 2, estimation of earthquake moment, released energy, and stress-strain drop from G wave spectrum, Bull. Earthquake Res. Inst., Tokyo Univ., 44, 73-88, 1966.

Aki, K., Scaling law of seismic spectrum, J. Geophys. Res., 72, 1217-1231, 1967.

Anderson, R.N., J.G. Sclater, Topography and evolution of the East Pacific Rise between 5°S and 20°S, Earth Planet. Sci. Lett., 14, 433-442, 1972.

Anderson, R.N., D.W. Forsyth, P. Molnar, J. Mammerickx, Fault plane solutions of earthquakes on the Nazca plate boundaries and the Easter plate, Earth Planet. Sci. Lett., 24, 188-202, 1974.

Bonatti, E. and J. Honnorez, Sections of the earth's crust in the equatorial Atlantic, J. Geophys. Res., 81, 4104-4116, 1976.

Brace, W.F. and J.D. Byerlee, California earthquakes: why only shallow focus?, Science, 168, 1573-1575, 1970.

Brune, J.N. and C.Y. King, Excitation of mantle Rayleigh waves of period 100 seconds as a function of magnitude, Bull. Seism. Soc. Am., 57, 1355-1365, 1967.

Brune, J.N., Seismic moment, seismicity and rate of slip along major fault zones, J. Geophys. Res., 73, 777-784, 1968.

Collette, B.J., J. Schouten, K. Rutten, and A.P. Slootweg, Structure of the Mid-Atlantic Ridge Province between 12° and 18°N, Marine Geophys. Res., 2, 143-179, 1974.

Davies, G.F. and J.N. Brune, Regional and global fault slip rates from seismicity, Nature Phys. Sci., 229, 101-107, 1971.

Fisher, R.L., J.G. Sclater, S.D. McKenzie, Evolution of the central Indian ridge, western Indian Ocean, Geol. Soc. Am. Bull., 82, 533-562, 1971.

Forsyth, D.W., Mechanisms of earthquakes and plate motions in the East Pacific, Earth Planet. Sci. Lett., 17, 189-193, 1972.

Forsyth, D.W., Anisotropy and the structural evolution of the oceanic upper mantle, Ph.D. Thesis, Mass. Inst. Tech., 1973.

Forsyth, D.W., Fault plane solutions and the tectonics of the South Atlantic and Scotia Sea, J. Geophys. Res., 80, 1429-1443, 1975.

Fox, P.J., E. Schreiber, H. Rowlett, and K. McCamy, The geology of the Oceanographer Fracture Zone: a model for fracture zones, J. Geophys. Res., 81, 4117-4128, 1976.

Geller, R.J., Scaling relations for earthquake source parameters and magnitudes, Bull. Seism. Soc. Am., 66, 1501-1523, 1976.

Geller, R.J. and H. Kanamori, Magnitudes of great shallow earthquakes from 1904 to 1952, to be published, 1977.

Gutenberg, B. and C.F. Richter, Earthquake magnitude, intensity, energy and acceleration, Bull. Seism. Soc. Am., 32, 163-191, 1942.

Gutenberg, B. and C.F. Richter, Seismicity of the Earth and Associated Phenomena, 2nd ed., Princeton Univ. Press, 1954.

Herron, E.M., Sea floor spreading and the Cenozoic history of the east-central Pacific, Geol. Soc. Am. Bull., 83, 1671-1685, 1972a.

Herron, E.M., Two small crustal plates in the South Pacific near Easter Island, Nature Phys. Sci., 240, 39-37, 1972b.

Kanamori, H. and G.S. Stewart, Mode of the strain release along the Gibbs Fracture Zone, Mid-Atlantic Ridge, Phys. Earth Planet. Int., 11, 312-332, 1976.

Keilis-Borok, V.I., Investigations of the mechanism of earthquakes, Sov. Res. Geophys. (Engl. transl.), 4, 29, 1960.

Klitgord, K.D., J.D. Mudie, P.A. Larson, and J. Grow, Fast sea floor spreading on the Chile ridge, Earth Planet. Sci. Lett., 20, 93-99, 1973.

Knopoff, L., Energy release in earthquakes, Geophys. J. Roy. Astron. Soc., 1, 44-52, 1958.

Madariaga, R., Implications of stress-drop models of earthquakes for the inversion of stress drop from seismic observations, Pure Appl. Geophys., to be published, 1977.

Mammerickx, J., R.N. Anderson, H.W. Menard, S.M. Smith, Morphology and tectonic evolution of the east-central Pacific, Geol. Soc. Am. Bull., 86, 111-118, 1975.

Minster, J.B., T.H. Jordan, P. Molnar, and E. Haines, Numerical modeling of instantaneous plate tectonics, Geophys. J. Roy. Astron. Soc., 36, 541-576, 1974.

Molnar, P., T. Atwater, J. Mammerickx, and S.M. Smith, Magnetic anomalies, bathymetry and the tectonic evolution of the South Pacific since late Cretaceous, Geophys. J. Roy. Astron. Soc., 40, 383, 420, 1975.

Norton, I.O., The present relative motion between Africa and Antarctica, Earth Planet. Sci. Lett., 33, 219-230, 1976.

Olivet, J., X. LePichon, S. Monti, and B. Sichler, Charlie-Gibbs Fracture Zone, J. Geophys. Res., 79, 2059-2072, 1974.

Richardson, R.M. and S.C. Solomon, Apparent stress and stress-drop for intraplate earthquakes and the magnitude of tectonic stress in the plates, Pure Appl. Geophys., to be published, 1977.

Rothe, J.P. The Seismicity of the Earth, UNESCO, 336 p., 1969.

Savage, J.C. and R.O. Burford, Discussion of a paper by C.H. Scholz and T.J. Fitch, Strain accumulation along the San Andreas fault, J. Geophys. Res., 76, 6469-6479, 1971.

Sclater, J.G., C. Bowin, R. Hey, H. Hoskins, J. Pierce, J. Phillips, and C. Tapscott, The Bouvet triple junction, J. Geophys. Res., 81, 1857-1869, 1976.

Shakal, A.F., Source mechanism discrimination for earthquakes of the Mid-Atlantic ridge, unpublished generals paper, 1975.

Sleep, N.H., Formation of oceanic crust: some thermal constraints, J. Geophys. Res., 80, 4037-4042, 1975.

Steskey, R.M., The mechanical behavior of faulted rocks at high temperatures and pressure, Sc.D. Thesis, Mass. Inst. Tech., 1975.

Sykes, L.R., Mechanism of earthquakes and nature of faulting on mid-oceanic ridges, J. Geophys. Res., 72, 2131-2153, 1967.

Thatcher, W., Strain accumulation on the northern San Andreas fault zone since 1906, J. Geophys. Res., 80, 4872-4880, 1975.

Thompson, G. and W. Melson, The petrology of oceanic crust across fracture zones in the Atlantic Ocean: evidence of a new kind of sea floor spreading, J. Geol., 80, 526-538, 1972.

Tsai, Y.B., Determination of focal depths of earthquakes in mid-oceanic ridges from amplitude spectra of surface waves, Ph.D. Thesis, Mass. Inst. Tech., 1969.

Tsai, Y.B. and K. Aki, Precise focal depth determination from amplitude spectra of surface waves, J. Geophys. Res., 75, 5729-5743, 1970.

Udias, A., Source parameters of earthquakes from spectra of Rayleigh waves, Geophys. J. Roy. Astron. Soc., 22, 353-376, 1971.

van Andel, T.H., D.K. Rea, R.P. Von Herzen, and H. Haskins, Ascension Fracture Zone, Ascension Island and the Mid-Atlantic Ridge, Geol. Soc. Am. Bull., 84, 1927-1956, 1973.

Vogt, P.R. and G.L. Johnson, Transform faults and longitudinal flow below the mid-oceanic ridge, J. Geophys. Res., 80, 1399-1428, 1975.

Weissel, J.K. and D.E. Hayes, Magnetic anomalies in the southeast Indian Ocean, Antarctic Oceanology II: the Austrialian-New Zealand Sector, ed. D.E. Hayes, Antarctic Research Series, 19, Am. Geophys. Un., 165-196, 1972.

Weidner, D. and K. Aki, Focal depth and mechanism of mid-oceanic ridge earthquakes, J. Geophys. Res., 78, 1818-1831, 1973.

Wyss, M., Apparent stresses of earthquakes on ridges compared to apparent stress of earthquakes in trenches, Geophys. J. Roy. Astron. Soc., 19, 479-484, 1970.

TABLE CAPTIONS

Table I) All of the transform data used in this study are listed by pole (see Table IV) and transform number. Velocity is in cm/yr, lengths and widths are in kilometers. For calculation of widths see text.

Table II) Data for all oceanic transforms which have had their source spectrum analyzed.

Table III) Detailed observations of moment and corner frequency for the six events studied in this thesis.

Table IV) List of plate boundaries listed by their associated pole numbers and letters used in Tables I and II, also Figures 1 through 13.

TABLE I.

| Pole | # | Lat. | Long. | L | V | 6.0 | | 6.2 | | 6.4 | | 6.6 | | 6.8 | | 7.0 | | 7.2 | | 7.4 | 7.5 | 7.9 | $W^1$ | $W^2$ | Name |
|---|---|---|---|---|---|---|---|---|---|---|---|---|---|---|---|---|---|---|---|---|---|---|---|---|---|
| 1 | 1 | 52N | 33W | 280, | 2,48 | 0 | 0 | 1 | 0 | 0 | 2 | 0 | 0 | 0 | 1 | 0 | 0 | 0 | 0 | 0 | 0 | 0 | 4,5 | 1,5 | GIBBS |
| 1 | 2 | 66N | 19W | 130, | 1,99 | 0 | 0 | 2 | 0 | 0 | 0 | 0 | 0 | 0 | 0 | 1 | 0 | 0 | 0 | 0 | 0 | 0 | 13,7 | 1,0 | TJORN |
| 2 | 1 | 24N | 45W | 130, | 3,17 | 0 | 0 | 1 | 0 | 1 | 2 | 0 | 0 | 0 | 0 | 0 | 1 | 0 | 0 | 0 | 0 | 0 | 15,2 | 0,9 | KANE |
| 2 | 2 | 30N | 42W | 70, | 2,95 | 1 | 0 | 1 | 0 | 0 | 0 | 0 | 0 | 0 | 0 | 0 | 0 | 0 | 0 | 0 | 0 | 0 | 1,4 | 0,6 | ATLANTIS |
| 2 | 3 | 35N | 36W | 140, | 2,74 | 3 | 0 | 1 | 1 | 0 | 0 | 0 | 0 | 0 | 0 | 0 | 0 | 0 | 0 | 0 | 0 | 0 | 2,0 | 1,0 | OCEANOGRAPHER |
| 3 | 1 | 44N | 128W | 350, | 5,50 | 5 | 1 | 2 | 2 | 0 | 2 | 0 | 1 | 0 | 0 | 0 | 0 | 0 | 0 | 0 | 0 | 0 | 1,7 | 1,1 | BLANCO |
| 3 | 2 | 49N | 129W | 160, | 5,28 | 3 | 1 | 2 | 1 | 0 | 2 | 1 | 0 | 0 | 0 | 0 | 0 | 0 | 0 | 0 | 0 | 0 | 3,0 | 0,8 | SOVANCO |
| 4 | 1 | 3S | 105W | 80, | 16,07 | 2 | 1 | 0 | 0 | 0 | 0 | 0 | 0 | 0 | 0 | 0 | 0 | 0 | 0 | 0 | 0 | 0 | 0,3 | 0,3 | |
| 4 | 2 | 4S | 102W | 60, | 16,17 | 0 | 1 | 1 | 0 | 0 | 1 | 0 | 0 | 0 | 0 | 0 | 0 | 0 | 0 | 0 | 0 | 0 | 0,6 | 0,3 | |
| 4 | 3 | 5S | 106W | 150, | 16,32 | 2 | 0 | 0 | 0 | 0 | 2 | 0 | 0 | 0 | 0 | 0 | 0 | 0 | 0 | 0 | 0 | 0 | 0,4 | 0,4 | |
| 4 | 4 | 9S | 109W | 120, | 16,96 | 3 | 0 | 1 | 1 | 0 | 0 | 0 | 0 | 0 | 0 | 0 | 0 | 0 | 0 | 0 | 0 | 0 | 0,4 | 0,3 | |
| 4 | 5 | 13S | 92W | 60, | 17,17 | 1 | 0 | 1 | 0 | 0 | 0 | 0 | 0 | 0 | 0 | 0 | 0 | 0 | 0 | 0 | 0 | 0 | 0,2 | 0,2 | |
| 4 | 6 | 28S | 113W | 200, | 18,22 | 2 | 0 | 3 | 0 | 0 | 1 | 0 | 0 | 0 | 0 | 0 | 0 | 0 | 0 | 0 | 0 | 0 | 0,3 | 0,4 | |
| 4 | 7 | 30S | 112W | 160, | 19,24 | 1 | 0 | 0 | 2 | 0 | 0 | 0 | 0 | 0 | 0 | 0 | 0 | 0 | 0 | 0 | 0 | 0 | 0,2 | 0,4 | |
| 5 | 1 | 2N | 91W | 200, | 5,93 | 2 | 0 | 0 | 0 | 0 | 2 | 0 | 0 | 0 | 0 | 0 | 0 | 0 | 0 | 0 | 0 | 0 | 0,9 | 0,8 | |
| 5 | 2 | 1N | 85W | 150, | 6,50 | 0 | 0 | 2 | 0 | 0 | 0 | 0 | 0 | 0 | 0 | 0 | 0 | 0 | 0 | 0 | 0 | 0 | 0,4 | 0,6 | |
| 6 | 1 | 7S | 68E | 180, | 3,73 | 1 | 0 | 1 | 0 | 0 | 0 | 0 | 0 | 0 | 0 | 0 | 0 | 0 | 0 | 0 | 0 | 0 | 0,4 | 1,0 | |
| 6 | 2 | 9S | 62E | 300, | 3,86 | 1 | 0 | 1 | 0 | 0 | 0 | 0 | 0 | 1 | 0 | 0 | 0 | 0 | 0 | 0 | 0 | 0 | 1,4 | 1,3 | |
| 6 | 3 | 14S | 68E | 130, | 4,18 | 2 | 0 | 0 | 0 | 0 | 0 | 0 | 0 | 0 | 0 | 0 | 0 | 0 | 0 | 0 | 0 | 0 | 0,4 | 0,8 | |
| 6 | 4 | 17S | 65E | 240, | 4,33 | 3 | 0 | 3 | 1 | 0 | 0 | 0 | 0 | 0 | 0 | 0 | 0 | 0 | 0 | 0 | 0 | 0 | 1,1 | 1,1 | |
| 6 | 5 | 19S | 65E | 110, | 4,50 | 0 | 0 | 1 | 0 | 0 | 0 | 0 | 0 | 0 | 0 | 0 | 0 | 0 | 0 | 0 | 0 | 0 | 0,4 | 0,7 | |
| 7 | 1 | 37S | 78E | 300, | 6,82 | 3 | 1 | 0 | 1 | 0 | 1 | 0 | 0 | 0 | 0 | 0 | 0 | 0 | 0 | 0 | 0 | 0 | 0,6 | 0,9 | |
| 7 | 2 | 41S | 69E | 240, | 7,01 | 0 | 0 | 2 | 0 | 0 | 1 | 0 | 1 | 0 | 0 | 0 | 0 | 0 | 0 | 0 | 0 | 0 | 1,0 | 0,8 | |
| 7 | 3 | 45S | 87E | 210, | 7,20 | 1 | 1 | 1 | 0 | 0 | 2 | 0 | 0 | 0 | 0 | 0 | 0 | 0 | 0 | 0 | 0 | 0 | 0,8 | 0,7 | |
| 7 | 4 | 46S | 98E | 240, | 7,46 | 1 | 0 | 0 | 1 | 0 | 0 | 0 | 1 | 0 | 0 | 1 | 0 | 0 | 0 | 0 | 0 | 0 | 2,5 | 0,8 | |
| 7 | 5 | 51S | 140E | 290, | 7,76 | 2 | 2 | 3 | 0 | 0 | 1 | 0 | 1 | 0 | 0 | 0 | 0 | 0 | 0 | 0 | 0 | 0 | 1,1 | 0,9 | |
| 7 | 6 | 52S | 141E | 200, | 7,73 | 4 | 0 | 0 | 1 | 0 | 0 | 0 | 0 | 0 | 0 | 0 | 0 | 0 | 0 | 0 | 0 | 0 | 0,5 | 0,7 | |
| 7 | 7 | 56S | 146E | 460, | 6,93 | 5 | 1 | 6 | 3 | 3 | 1 | 0 | 1 | 0 | 0 | 0 | 0 | 0 | 0 | 0 | 0 | 0 | 1,5 | 1,1 | |
| 7 | 8 | 60S | 149E | 260, | 6,90 | 2 | 0 | 3 | 0 | 0 | 4 | 0 | 0 | 0 | 0 | 0 | 0 | 0 | 0 | 0 | 0 | 0 | 1,4 | 0,8 | |
| 7 | 9 | 62S | 154E | 360, | 6,82 | 1 | 1 | 1 | 2 | 1 | 1 | 0 | 0 | 0 | 0 | 0 | 1 | 0 | 0 | 0 | 0 | 0 | 2,7 | 1,0 | |
| 9 | 1 | 6N | 104W | 170, | 12,40 | 2 | 0 | 1 | 0 | 0 | 0 | 1 | 0 | 0 | 0 | 0 | 0 | 0 | 0 | 0 | 0 | 0 | 0,5 | 0,5 | |
| 9 | 2 | 10N | 104W | 160, | 11,58 | 2 | 0 | 1 | 0 | 0 | 0 | 1 | 1 | 0 | 0 | 0 | 0 | 0 | 0 | 0 | 0 | 0 | 1,0 | 0,5 | |
| 9 | 3 | 15N | 105W | 130, | 9,92 | 1 | 0 | 1 | 0 | 0 | 0 | 0 | 0 | 0 | 0 | 0 | 0 | 0 | 0 | 0 | 0 | 0 | 0,2 | 0,5 | |
| 10 | 1 | 52S | 115W | 250, | 7,76 | 2 | 0 | 1 | 1 | 0 | 1 | 0 | 0 | 0 | 0 | 0 | 0 | 0 | 0 | 0 | 0 | 0 | 0,4 | 0,7 | MENARD |
| 10 | 2 | 56S | 123W | 400, | 8,95 | 1 | 0 | 2 | 0 | 1 | 2 | 1 | 0 | 0 | 0 | 1 | 0 | 0 | 0 | 0 | 0 | 0 | 1,5 | 0,9 | HEEZEN |
| 10 | 3 | 55S | 132W | 530, | 9,84 | 5 | 2 | 2 | 2 | 0 | 4 | 0 | 1 | 1 | 0 | 0 | 0 | 0 | 0 | 0 | 0 | 0 | 1,2 | 1,1 | ELTANIN |
| 10 | 4 | 57S | 141W | 370, | 8,37 | 1 | 0 | 2 | 0 | 1 | 1 | 0 | 0 | 0 | 0 | 0 | 0 | 0 | 0 | 0 | 0 | 0 | 0,4 | 0,9 | UDINTSEV |
| 10 | 5 | 59S | 160W | 320, | 7,28 | 0 | 0 | 0 | 0 | 0 | 0 | 0 | 0 | 0 | 0 | 0 | 0 | 1 | 0 | 0 | 0 | 0 | 3,2 | 0,9 | |
| 10 | 6 | 63S | 166W | 260, | 6,56 | 1 | 0 | 1 | 0 | 0 | 0 | 0 | 0 | 0 | 0 | 0 | 0 | 0 | 0 | 0 | 0 | 0 | 0,2 | 0,9 | |
| 11 | 1 | 54S | 3W | 150, | 3,69 | 0 | 0 | 2 | 0 | 0 | 0 | 0 | 0 | 0 | 0 | 0 | 0 | 0 | 0 | 0 | 0 | 0 | 0,6 | 0,9 | |
| 11 | 2 | 47S | 15W | 290, | 3,91 | 1 | 0 | 0 | 0 | 0 | 0 | 0 | 0 | 0 | 0 | 0 | 1 | 0 | 0 | 0 | 0 | 0 | 4,4 | 1,3 | |
| 11 | 3 | 37S | 18W | 180, | 4,04 | 1 | 0 | 2 | 0 | 0 | 1 | 0 | 0 | 0 | 0 | 0 | 0 | 0 | 0 | 0 | 0 | 0 | 1,2 | 1,0 | |
| 11 | 4 | 36S | 15W | 140, | 4,05 | 0 | 2 | 0 | 0 | 0 | 1 | 0 | 0 | 0 | 0 | 0 | 0 | 0 | 0 | 0 | 0 | 0 | 1,2 | 0,9 | |
| 11 | 5 | 12S | 14W | 130, | 3,34 | 2 | 0 | 1 | 0 | 0 | 0 | 0 | 0 | 0 | 0 | 0 | 0 | 0 | 0 | 0 | 0 | 0 | 0,8 | 0,8 | |
| 11 | 6 | 5S | 12W | 220, | 3,70 | 1 | 0 | 1 | 0 | 0 | 0 | 0 | 0 | 0 | 0 | 0 | 0 | 0 | 0 | 0 | 0 | 0 | 0,4 | 1,1 | |
| 11 | 7 | 1S | 15W | 340, | 3,56 | 2 | 0 | 0 | 1 | 0 | 4 | 0 | 0 | 0 | 0 | 0 | 0 | 1 | 0 | 0 | 0 | 0 | 7,9 | 1,5 | CHAIN |
| 11 | 8 | 0N | 27W | 950, | 3,48 | 3 | 2 | 6 | 1 | 2 | 2 | 0 | 1 | 1 | 0 | 1 | 1 | 0 | 0 | 0 | 0 | 0 | 4,1 | 2,5 | ROMANCHE |
| 11 | 9 | 1N | 28W | 610, | 3,39 | 4 | 0 | 3 | 3 | 1 | 4 | 0 | 0 | 0 | 1 | 0 | 0 | 0 | 0 | 0 | 0 | 0 | 2.8 | 2,0 | ST. PAULS |
| 11 | 10 | 7N | 36W | 510, | 3,09 | 5 | 0 | 0 | 0 | 0 | 2 | 1 | 0 | 0 | 1 | 0 | 1 | 0 | 0 | 1 | 0 | 0 | 16,8 | 1,9 | |
| 11 | 11 | 8N | 39W | 140, | 3,05 | 0 | 0 | 0 | 0 | 0 | 0 | 0 | 1 | 0 | 0 | 1 | 0 | 0 | 0 | 0 | 0 | 0 | 9,5 | 1,0 | |
| 11 | 12 | 11N | 43W | 330, | 2,92 | 0 | 0 | 0 | 1 | 0 | 0 | 0 | 0 | 0 | 1 | 1 | 0 | 1 | 0 | 0 | 1 | 0 | 41,0 | 1,6 | VEMA |
| 11 | 13 | 13N | 44W | 80, | 2,86 | 2 | 0 | 0 | 0 | 0 | 0 | 0 | 0 | 0 | 0 | 0 | 0 | 0 | 0 | 0 | 0 | 0 | 1,0 | 0,7 | |
| 11 | 14 | 15N | 46W | 160, | 2,73 | 2 | 0 | 0 | 0 | 1 | 1 | 0 | 0 | 0 | 0 | 0 | 0 | 0 | 0 | 0 | 0 | 0 | 1,9 | 1,2 | |
| 12 | 1 | 56S | 2W | 220, | 2,37 | 0 | 1 | 1 | 0 | 0 | 0 | 0 | 0 | 0 | 1 | 0 | 1 | 0 | 0 | 0 | 0 | 0 | 14,1 | 1,3 | CONRAD |
| 12 | 2 | 59S | 12W | 450, | 2,33 | 1 | 0 | 0 | 1 | 0 | 3 | 0 | 2 | 0 | 1 | 0 | 0 | 0 | 0 | 0 | 0 | 0 | 3,6 | 2,4 | |
| 12 | 3 | 61S | 20W | 80, | 2,29 | 1 | 0 | 0 | 0 | 0 | 0 | 0 | 0 | 0 | 0 | 0 | 0 | 0 | 0 | 0 | 0 | 0 | 0,6 | 0,8 | |
| 13 | 1 | 49S | 32E | 400, | 1,55 | 0 | 0 | 0 | 0 | 0 | 0 | 0 | 0 | 0 | 0 | 0 | 0 | 0 | 0 | 0 | 0 | 1 | 219,3 | 2,0 | |
| 14 | 1 | 36S | 98W | 270, | 7,10 | 2 | 0 | 2 | 0 | 0 | 2 | 0 | 0 | 0 | 0 | 0 | 0 | 0 | 0 | 0 | 0 | 0 | 0,7 | 0,8 | |
| 14 | 2 | 36S | 97W | 160, | 7,19 | 1 | 0 | 0 | 0 | 0 | 1 | 0 | 0 | 0 | 0 | 0 | 0 | 0 | 0 | 0 | 0 | 0 | 0,5 | 0,6 | |
| 14 | 3 | 41S | 69W | 280, | 7,32 | 2 | 0 | 0 | 0 | 0 | 0 | 0 | 0 | 0 | 0 | 0 | 0 | 0 | 0 | 0 | 0 | 0 | 0,1 | 0,9 | |

$W^1$-width Brune's method

$W^2$-mean depth of 100°C isotherm

TABLE II.

| DA | MO | YR | LAT | LONG | POLE | #. | $M_S$[1] | USCGS | ISC | MOMENT[2] | REF[3] | ησ-M[4] | ησ-ISC[4] |
|---|---|---|---|---|---|---|---|---|---|---|---|---|---|
| 16 | 10 | 74 | 52.60N | 32.10W | 1 | 1 | 6.9& | 0.0 | 5.7 | 45.00 | 1 | 10.36 | 0.02 |
| 13 | 2 | 67 | 52.70N | 34.10W | 1 | 1 | 6.5& | 5.6 | 5.6 | 34.00 | 1 | 3.44 | 0.02 |
| 28 | 3 | 63 | 66.29N | 19.78W | 1 | 2 | 7.0* | 0.0 | 0.0 | 27.60 | 5 | 23.86 | 0.0 |
| 19 | 5 | 63 | 23.80N | 45.96W | 2 | 1 | 6.4* | 0.0 | 0.0 | 24.96 | 5 | 0.0 | 0.0 |
| 17 | 5 | 64 | 35.30N | 36.07W | 2 | 3 | 5.8* | 5.6 | 5.6 | 1.94 | 6 | 0.0 | 0.30 |
| 22 | 8 | 63 | 42.80N | 126.18W | 3 | 1 | 5.7* | 0.0 | 0.0 | 0.81 | 5 | 0.0 | 0.0 |
| 20 | 6 | 65 | 42.93N | 126.29W | 3 | 1 | 5.7* | 5.6 | 5.5 | 0.19 | 3 | 0.0 | 1.74 |
| 7 | 7 | 64 | 43.35N | 127.20W | 3 | 1 | 0.0 | 5.7 | 5.1 | 0.04 | 3 | 0.0 | 0.90 |
| 14 | 6 | 65 | 44.50N | 129.50W | 3 | 1 | 0.0 | 5.4 | 5.0 | 0.16 | 3 | 0.0 | 0.13 |
| 1 | 10 | 64 | 43.40N | 126.60W | 3 | 1 | 0.0 | 0.0 | 5.1 | 0.16 | 3 | 0.0 | 0.23 |
| 22 | 5 | 66 | 21.26N | 108.70W | 3 | 0 | 0.0 | 5.3 | 5.2 | 0.20 | 3 | 0.0 | 0.31 |
| 23 | 5 | 66 | 21.36N | 108.60W | 3 | 0 | 0.0 | 5.4 | 5.2 | 0.31 | 3 | 0.0 | 0.20 |
| 9 | 9 | 69 | 4.43S | 105.90W | 4 | 3 | 5.3& | 5.2 | 4.9 | 0.48 | 2 | 0.0 | 0.02 |
| 13 | 11 | 70 | 23.72S | 112.72W | 4 | 6 | 5.8& | 5.6 | 5.4 | 1.37 | 2 | 0.0 | 0.14 |
| 12 | 10 | 64 | 31.40S | 110.80W | 4 | 7 | 6.2* | 5.9 | 0.0 | 2.40 | 2 | 0.0 | 0.0 |
| 7 | 3 | 63 | 26.87S | 113.60W | 4 | 0 | 6.5* | 0.0 | 0.0 | 7.64 | 2 | 15.33 | 0.0 |
| 3 | 11 | 65 | 22.34S | 114.00W | 4 | 0 | 6.0* | 5.8 | 5.8 | 1.94 | 2 | 0.0 | 0.89 |
| 6 | 11 | 65 | 22.13S | 113.80W | 4 | 0 | 6.2* | 6.2 | 5.7 | 0.96 | 2 | 0.0 | 1.04 |
| 26 | 6 | 69 | 2.01N | 90.48W | 5 | 1 | 5.3& | 5.0 | 5.0 | 0.60 | 2 | 0.0 | 0.03 |
| 6 | 4 | 66 | 45.80S | 96.10E | 7 | 4 | 0.0 | 5.7 | 5.7 | 3.80 | 3 | 0.0 | 0.26 |
| 17 | 2 | 66 | 32.20S | 78.90E | 7 | 0 | 0.0 | 6.4 | 6.0 | 9.40 | 3 | 0.0 | 0.56 |
| 19 | 12 | 65 | 32.20S | 78.80E | 7 | 0 | 5.9* | 5.7 | 5.5 | 1.40 | 3 | 0.0 | 0.24 |
| 6 | 12 | 65 | 18.87N | 107.20W | 9 | 0 | 6.7* | 5.9 | 5.7 | 13.72 | 3 | 17.03 | 0.07 |
| 21 | 1 | 67 | 49.70S | 114.90W | 10 | 1 | 0.0 | 5.4 | 5.4 | 3.96 | 2 | 0.0 | 0.05 |
| 4 | 4 | 71 | 56.60S | 122.50W | 10 | 2 | 6.6& | 6.2 | 5.7 | 8.00 | 7 | 20.67 | 0.12 |
| 18 | 8 | 69 | 56.00S | 123.40W | 10 | 2 | 6.4& | 5.1 | 5.3 | 1.70 | 7 | 0.0 | 0.06 |
| 3 | 4 | 63 | 54.40S | 128.20W | 10 | 2 | 6.5* | 0.0 | 0.0 | 1.33 | 3 | 88.03 | 0.0 |
| 9 | 9 | 67 | 54.80S | 136.00W | 10 | 3 | 6.1& | 5.4 | 5.1 | 3.40 | 7 | 0.0 | 0.01 |
| 24 | 8 | 70 | 56.60S | 142.50W | 10 | 4 | 6.4& | 5.9 | 5.8 | 4.40 | 7 | 0.0 | 0.39 |
| 14 | 12 | 64 | 54.30S | 2.40W | 11 | 1 | 6.2* | 0.0 | 5.7 | 7.99 | 3 | 0.0 | 0.12 |
| 16 | 8 | 65 | 0.50S | 20.00W | 11 | 8 | 6.4* | 6.2 | 6.0 | 2.76 | 3 | 0.0 | 1.89 |
| 15 | 11 | 65 | 0.20S | 18.70W | 11 | 8 | 6.4* | 5.8 | 5.7 | 2.03 | 3 | 0.0 | 0.49 |
| 3 | 8 | 63 | 7.79N | 35.80W | 11 | 10 | 6.8$ | 6.1 | 0.0 | 12.20 | 4 | 27.05 | 0.0 |
| 17 | 11 | 63 | 7.80N | 37.40W | 11 | 10 | 6.5$ | 0.0 | 0.0 | 3.83 | 4 | 30.57 | 0.0 |
| 19 | 6 | 70 | 15.40N | 45.90W | 11 | 14 | 5.8& | 5.5 | 5.5 | 1.03 | 6 | 0.0 | 0.32 |
| 10 | 11 | 42 | 49.50S | 32.00E | 13 | 1 | 7.9% | 0.0 | 0.0 | 2800.00 | 8 | 5.26 | 0.0 |
| 8 | 6 | 68 | 48.70S | 31.50E | 13 | 0 | 6.0& | 5.6 | 5.6 | 2.50 | 7 | 0.0 | 0.23 |
| 8 | 1 | 74 | 38.90S | 46.20E | 13 | 0 | 6.1& | 6.0 | 5.9 | 1.80 | 7 | 0.0 | 1.67 |
| 19 | 4 | 64 | 41.73S | 34.06W | 14 | 3 | 0.0 | 5.5 | 5.4 | 0.94 | 2 | 0.0 | 0.20 |
| 6 | 10 | 64 | 36.20S | 100.90W | 14 | 1 | 0.0 | 5.5 | 5.2 | 2.93 | 2 | 0.0 | 0.02 |

**KEY**

1) Reference for Magnitudes

* Rothe (1969)

& U.S.C.G.S.

$ Udias (1971)

% Gutenberg & Richter (1954)

2) $10^{25}$ dyne/cm

3) References for Moment

1 - Kanamori and Stewart (1976)

2 - Forsyth (1973)

3 - Tsai (1969)

4 - Udias (1971)

5 - Wyss (1970)

6 - Weidner and Aki (1973)

7 - this study

8 - Brune and King (1967)

4) Apparent stress in bars

TABLE III.

| Date | Station | $M_o$* | $f_o$ Hz. | |
|---|---|---|---|---|
| 09-09-67 | SBA | 5.0 | .032 | |
| | WEL | 2.9 | .030 | |
| | RAR | 2.1 | .040 | |
| | AFI | 3.4 | .028 | mean $M_o$ = 3.0 |
| | PEL | 5.4 | .040 | mean $f_o$ = .030 |
| | HNR | 3.0 | .020 | $\Delta\sigma$ = $823/w^2$ bars |
| | MUN | 2.9 | .030 | |
| | RAB | 2.9 | .022 | |
| | PMG | 3.5 | .025 | |
| 24-08-70 | RAR | 3.6 | .050 | |
| | PEL | 4.8 | .025 | mean $M_o$ = 4.4 |
| | PMG | 5.0 | .045 | mean $f_o$ = .045 |
| | RAB | 4.2 | .050 | $\Delta\sigma$ = $1616/w^2$ bars |
| 04-04-71 | RAR | 6.1 | .040 | |
| | LPA | 9.8 | .620 | |
| | QUI | 7.0 | .040 | mean $M_o$ = 8.0 |
| | BOG | 9.1 | .025 | mean $f_o$ = .031 |
| | BHP | 6.2 | .020 | |
| | LPS | 7.1 | .039 | $\Delta\sigma$ = $2024/w^2$ bars |
| | MUN | 10.5 | .040 | |
| 18-8-69 | PEL | 1.7 | .040 | |
| | LPA | 2.4 | .020 | mean $M_o$ = 1.7 |
| | NNA | 1.5 | .060 | mean $f_o$ = .037 |
| | BHP | 1.2 | .030 | $\Delta\sigma$ = $513/w^2$ bars |
| 08-06-68 | NAI | 3.0 | .025 | |
| | AAE | 2.8 | .040 | mean $M_o$ = 2.5 |
| | MUN | 2.1 | .030 | mean $f_o$ = .029 |
| | NAT | 2.0 | .020 | $\Delta\sigma$ = $591/w^2$ bars |
| 08-01-74 | AAE | 3.0 | .050 | |
| | SPA | 1.5 | .080 | mean $M_o$ = 1.8 |
| | MUN | 1.7 | .025 | mean $f_o$ = .032 |
| | SHI | 1.3 | .080 | $\Delta\sigma$ = $470/w^2$ bars |
| | ADE | 1.5 | .025 | |

* $M_o$ (dyne cm) x $10^{25}$

TABLE IV.

| Table I | Figures | Plate Boundary |
|---|---|---|
| 1 | A | EUR/NAM |
| 2 | B | AFR/NAM |
| 3 | N | NAM/PAC |
| 4 | P | NAZ/PAC |
| 5 | K | NAZ/COC |
| 6 | E | IND/AFR |
| 7 | F | IND/ANT |
| 9 | T | COC/PAC |
| 10 | S | PAC/ANT |
| 11 | C | AFR/SAM |
| 12 | V | SAM/ANT |
| 13 | D | AFR/ANT |
| 14 | X | ANT/NAZ |

FIGURE CAPTIONS

Figure 1) Plot of $M_o$ vs. $M_s$ using earthquakes in Table II with U.S.C.G.S. magnitudes, $M_s$ by Udias (1975) and the magnitude 7.9 event on the Africa-Antarctic ridge. Dotted lines are $\omega^2$ and $\omega^2$ models of Aki (1967) as plotted by Brune and King (1967). Definition of letters are in Table IV.

Figure 2) Plot of $M_o$ vs. $M_s$ using all earthquakes in Table II with a moment derived from source spectra and a reported magnitude (symbols from Table IV). Dotted lines are $\omega^2$ and $\omega^3$ models of Aki (1967) as plotted by Brune and King (1967).

Figure 3) Plot of $M_o$ vs. spreading rate using moments from Table I (symbols from Table IV).

Figure 4) Plot of $M_o$ vs. spreading rate using magnitudes from Table I and the moment-magnitude relation given by the $\omega^2$ model in Figure 1.

Figure 5) Plot of moment sum vs. spreading rate using magnitudes from Table I and the moment-magnitudes relation given by the $\omega^2$ model in Figure 1.

Figure 6) Plot of $M_o$ vs. transform length using the earthquakes in Table II.

Figure 7) Plot of $M_o$ vs. transform length using magnitudes from Table I and converting to moments using the $\omega^2$ model in Figure 1.

Figure 8) Plot of moment vs. transform length using magnitudes from Table I and converting to moments using the $\omega^2$ model in Figure 1.

Figure 9) Plot of effective transform width vs. transform length. Dotted lines show trend of transforms with similar spreading rates.

Figure 10) Plot of effective transform width vs. spreading rate.

Figure 11) Plot of transform length vs. slip rate.

Figure 12) Plot of $m_b$ vs. $M_s$ for transform earthquakes, where $m_b$ is from U.S.C.G.S.

Figure 13) Plot of $m_b$ vs. $M_s$ for transform earthquakes, where $m_b$ is from I.S.C.

Figure 14) Possible bounds of transform area undergoing brittle failure for a transform of length 300 km and a spreading rate of 10 cm/year.

Figure 15) Predicted magnitude-moment relations based on least-squares representation of the results of inversion of slip rate and magnitude data from 57 transforms. Each line represents a different isotherm used to determine the fault area as in Figure 14a. Data are from Figure 1.

Figure 16) Discrete solution for 57 transforms and four isotherms. The area as in Figure 14a is used.

Figure 17) Discrete solution for 49 selected transforms (see text) and four isotherms.

Figure 18) Least-squares solution for 49 transforms and four isotherms.

Figure 19) Least-squares solution for 57 transforms using an area as in Figure 14b.

Figure 20) Earthquakes of magnitude 6.0 and greater occurring on the Romanche Transform.

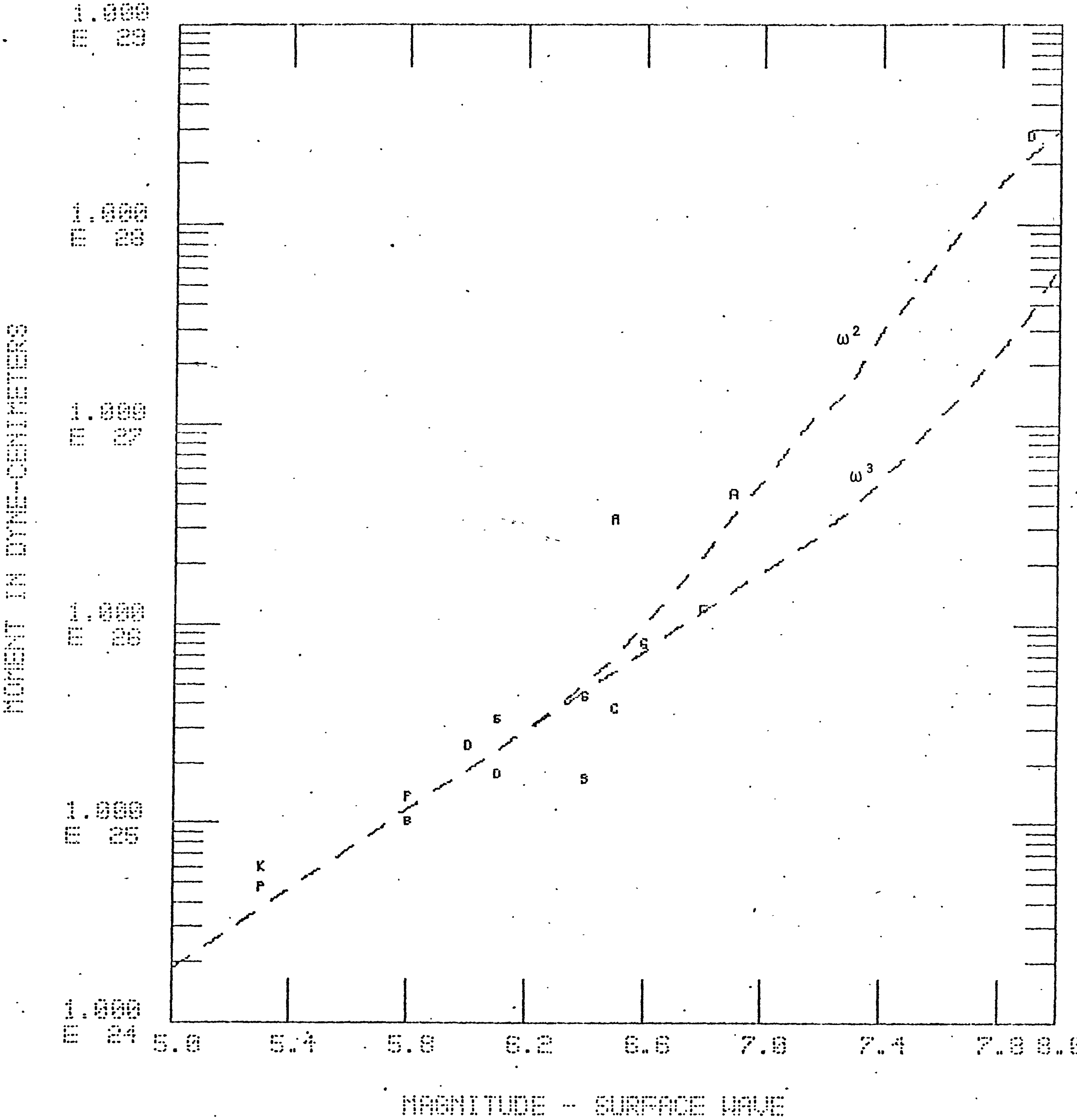

1.000 E 29
1.000 E 28
1.000 E 27
1.000 E 26
1.000 E 25
1.000 E 24
MOMENT IN DYNE-CENTIMETERS
5.0
5.4
5.8
6.2
6.6
7.0
7.4
7.8
8.0
MAGNITUDE - SURFACE WAVE
$\omega^2$
$\omega^3$


Figure 1

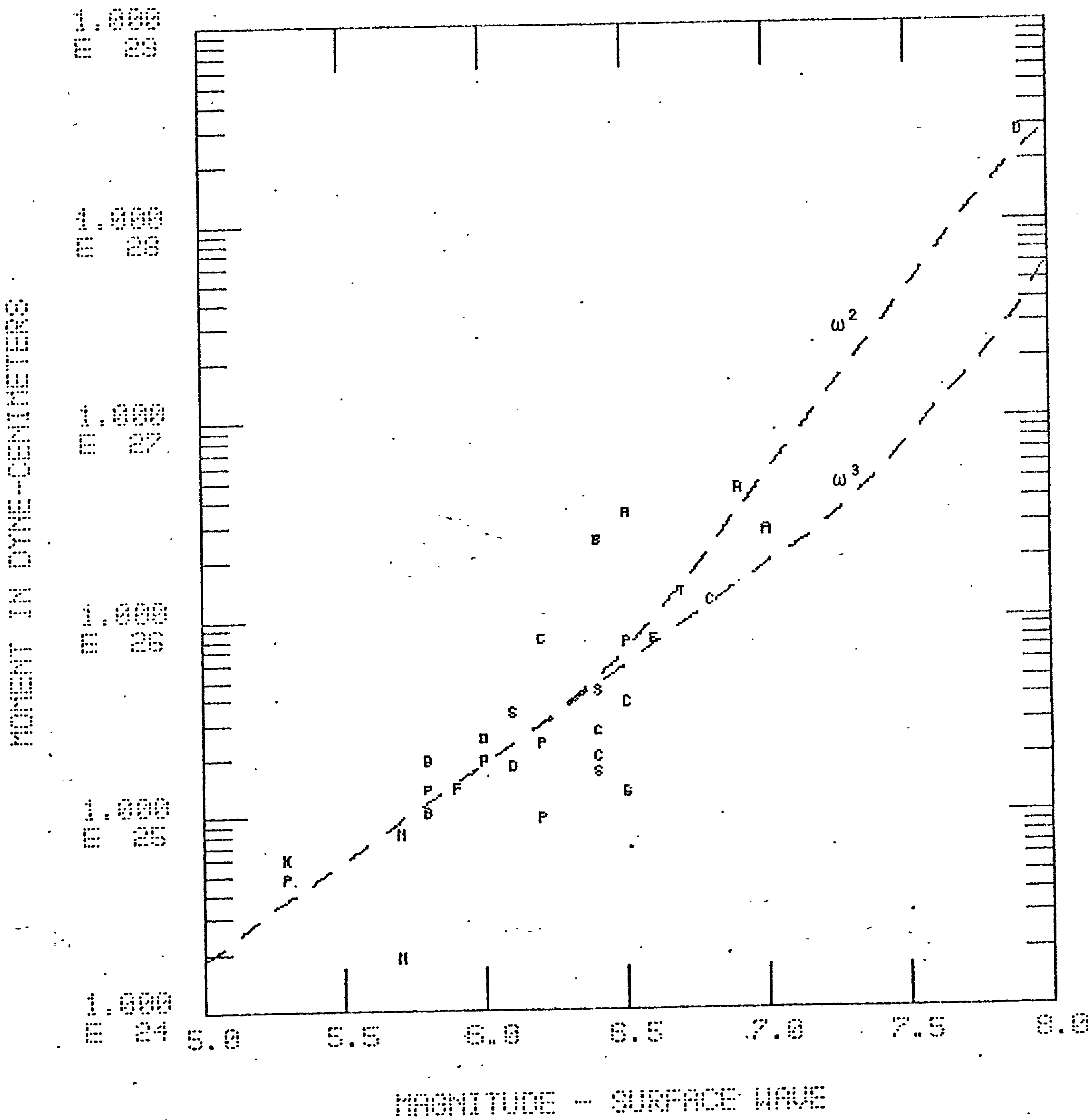
MOMENT IN DYNE-CENTIMETERS
1.000 E 29
1.000 E 28
1.000 E 27
1.000 E 26
1.000 E 25
1.000 E 24
5.0
5.5
6.0
6.5
7.0
7.5
8.0
MAGNITUDE - SURFACE WAVE
ω2
ω3

Figure 2

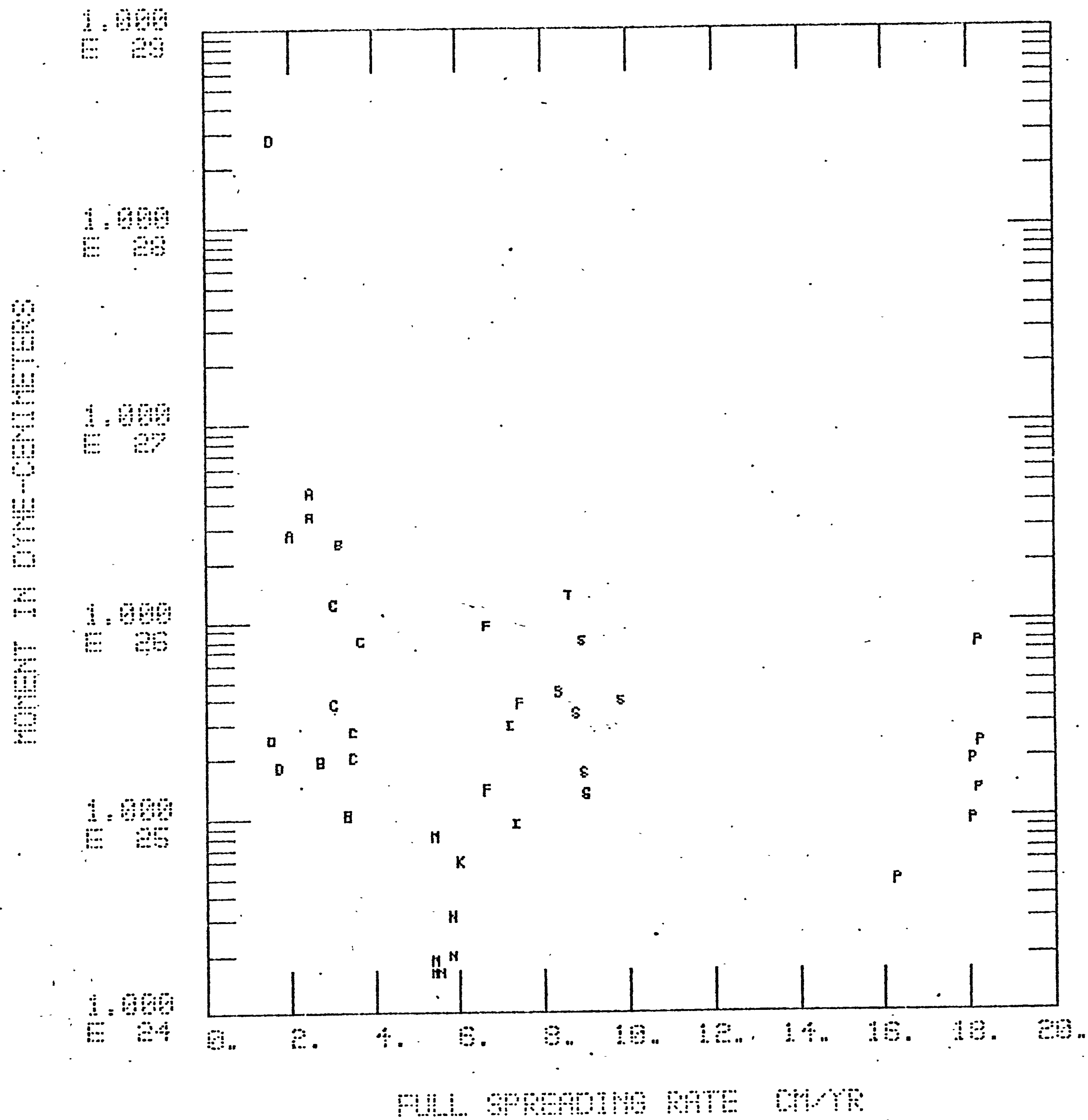
1.000 E 29
1.000 E 28
1.000 E 27
1.000 E 26
1.000 E 25
1.000 E 24
MOMENT IN DYNE-CENTIMETERS
0. 2. 4. 6. 8. 10. 12. 14. 16. 18. 20.
FULL SPREADING RATE CM/YR
D
A
A
A
B
C
C
C
C
C
D
D
B
B
F
F
F
T
S
S
S
S
S
S
S
I
I
N
K
N
N
N
NN
P
P
P
P
P
P

Figure 3

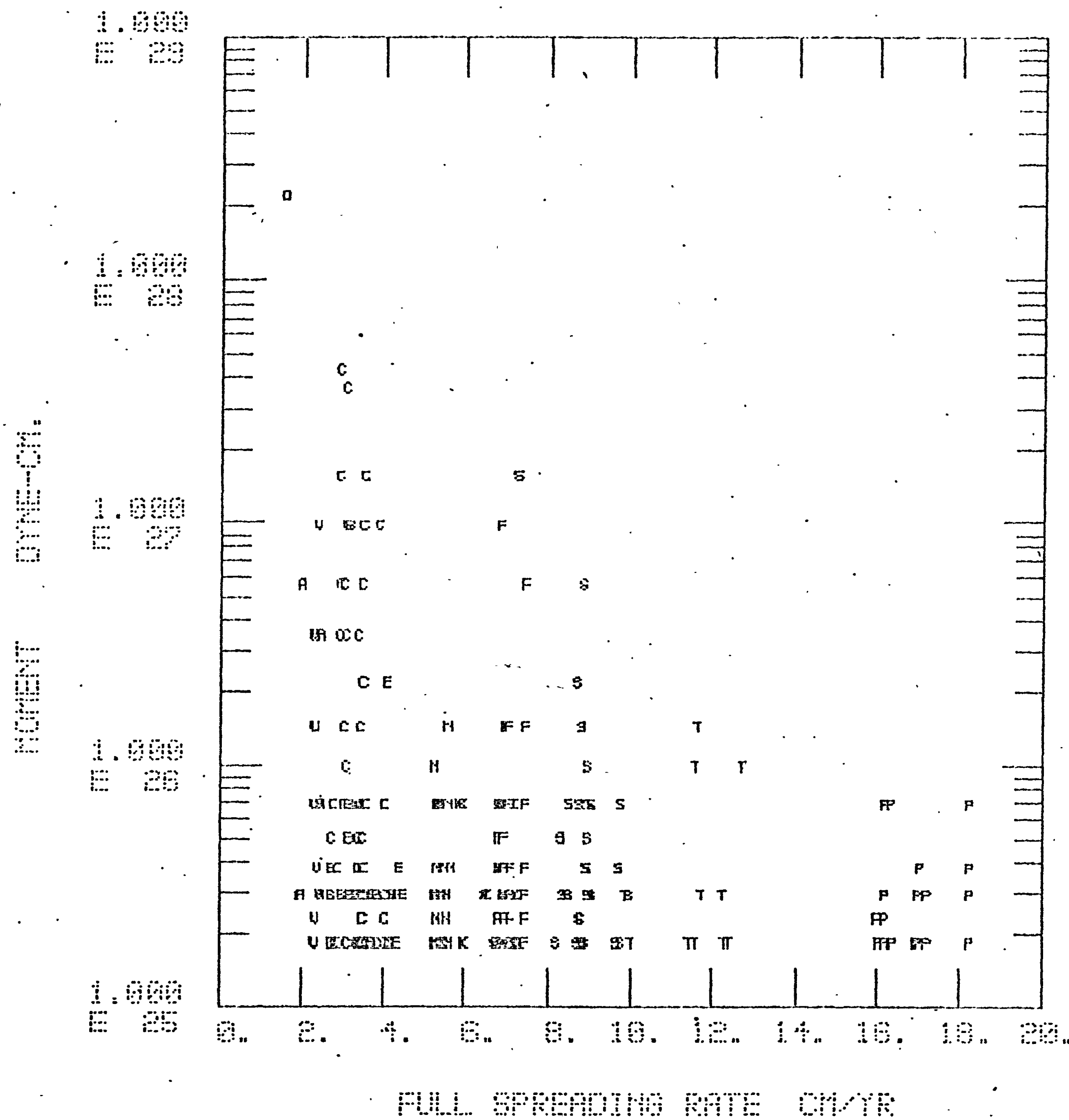

1.000 E 29
1.000 E 28
1.000 E 27
1.000 E 26
1.000 E 25
MOMENT DYNE-CM.
0.
2.
4.
6.
8.
10.
12.
14.
16.
18.
20.
FULL SPREADING RATE CM/YR


Figure 4

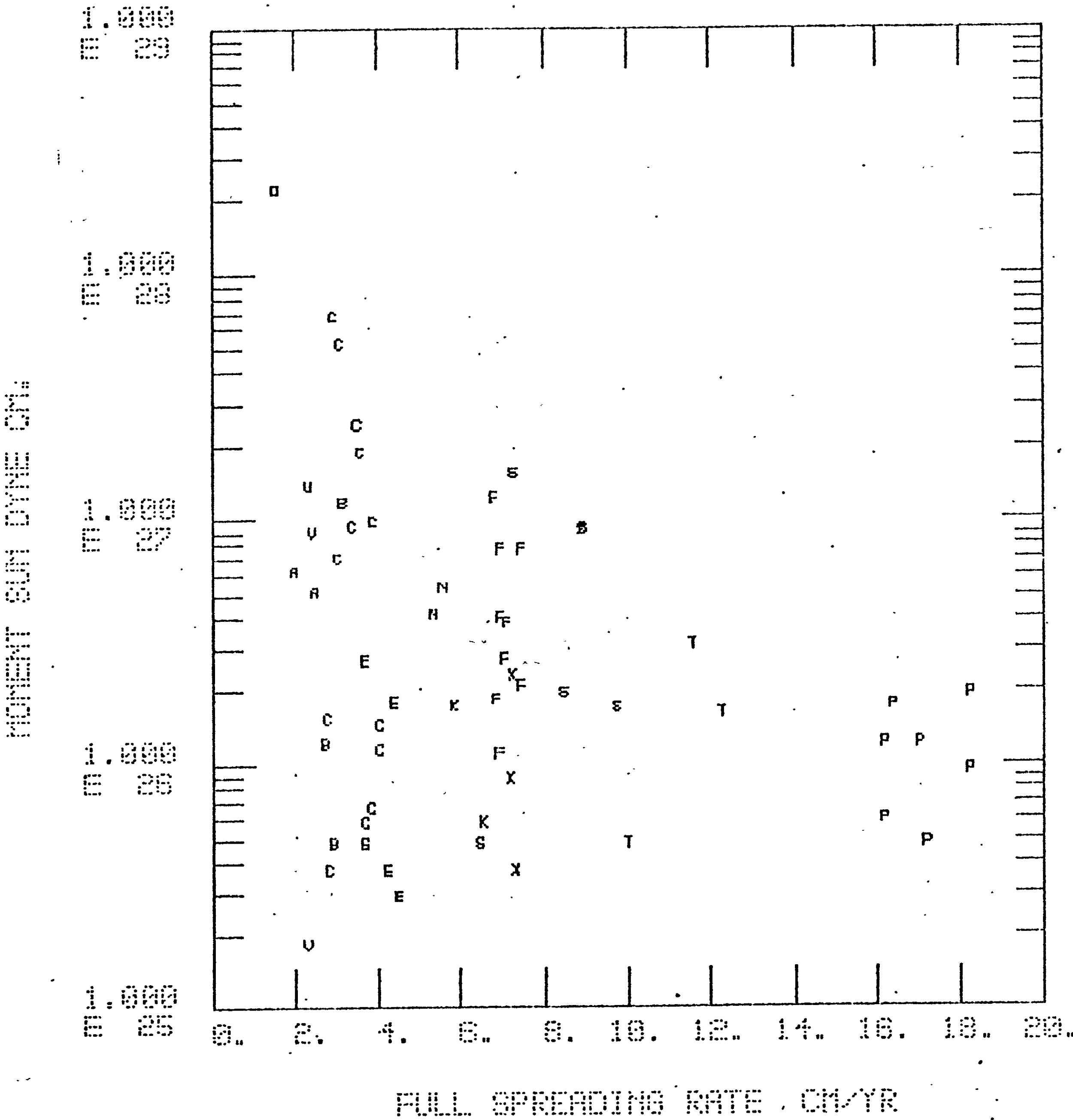
1.000
E 29
1.000
E 28
1.000
E 27
1.000
E 26
1.000
E 25
MOMENT SUM DYNE CM.
0.
2.
4.
6.
8.
10.
12.
14.
16.
18.
20.
FULL SPREADING RATE , CM/YR

Figure 5

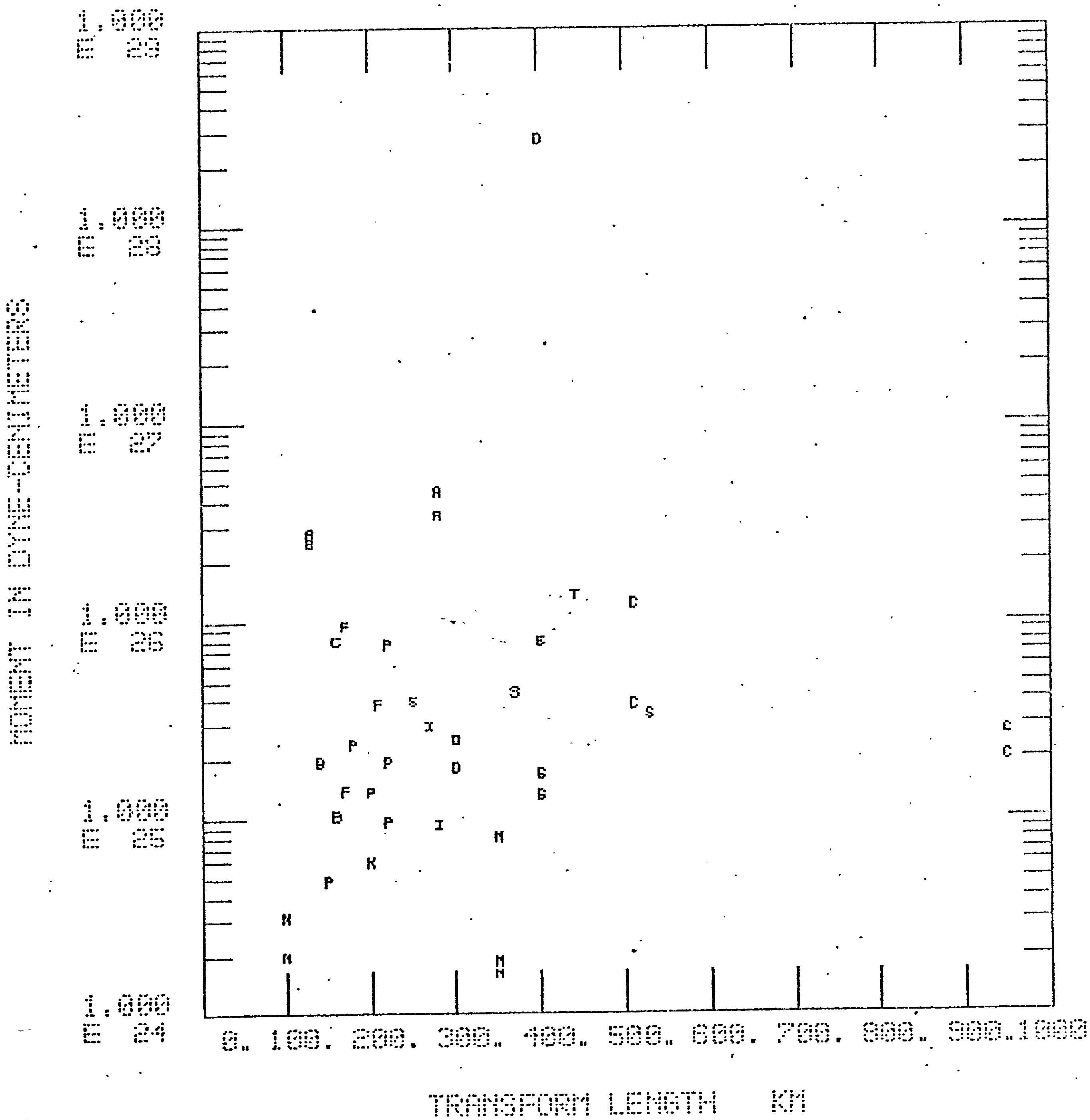
1.000 E 29
1.000 E 28
1.000 E 27
1.000 E 26
1.000 E 25
1.000 E 24
MOMENT IN DYNE-CENTIMETERS
0. 100. 200. 300. 400. 500. 600. 700. 800. 900. 1000.
TRANSFORM LENGTH KM

Figure 6

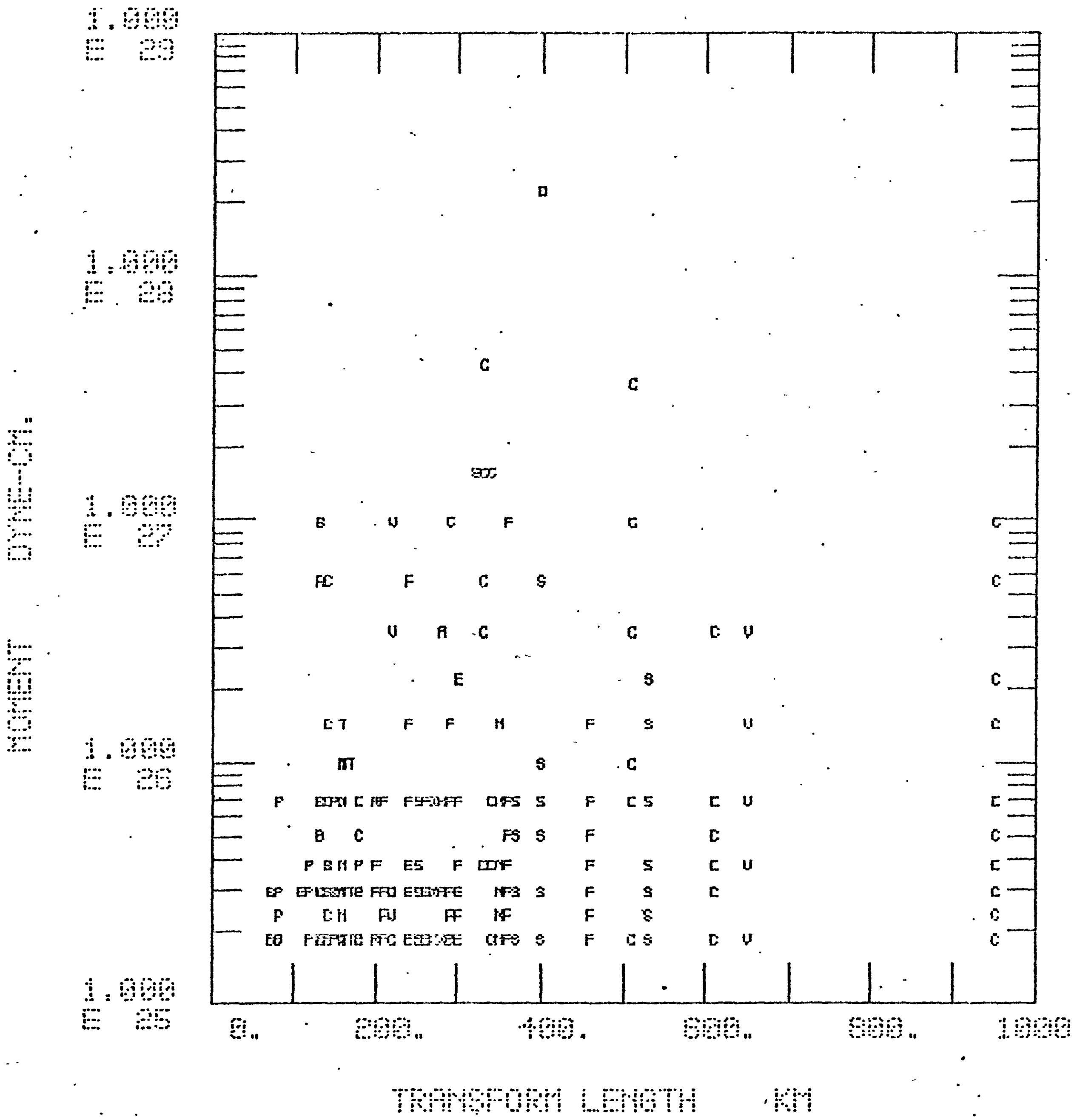
1.000 E 29
1.000 E 28
1.000 E 27
1.000 E 26
1.000 E 25
MOMENT DYNE-CM.
0.
200.
400.
600.
800.
1000.
TRANSFORM LENGTH KM

Figure 7

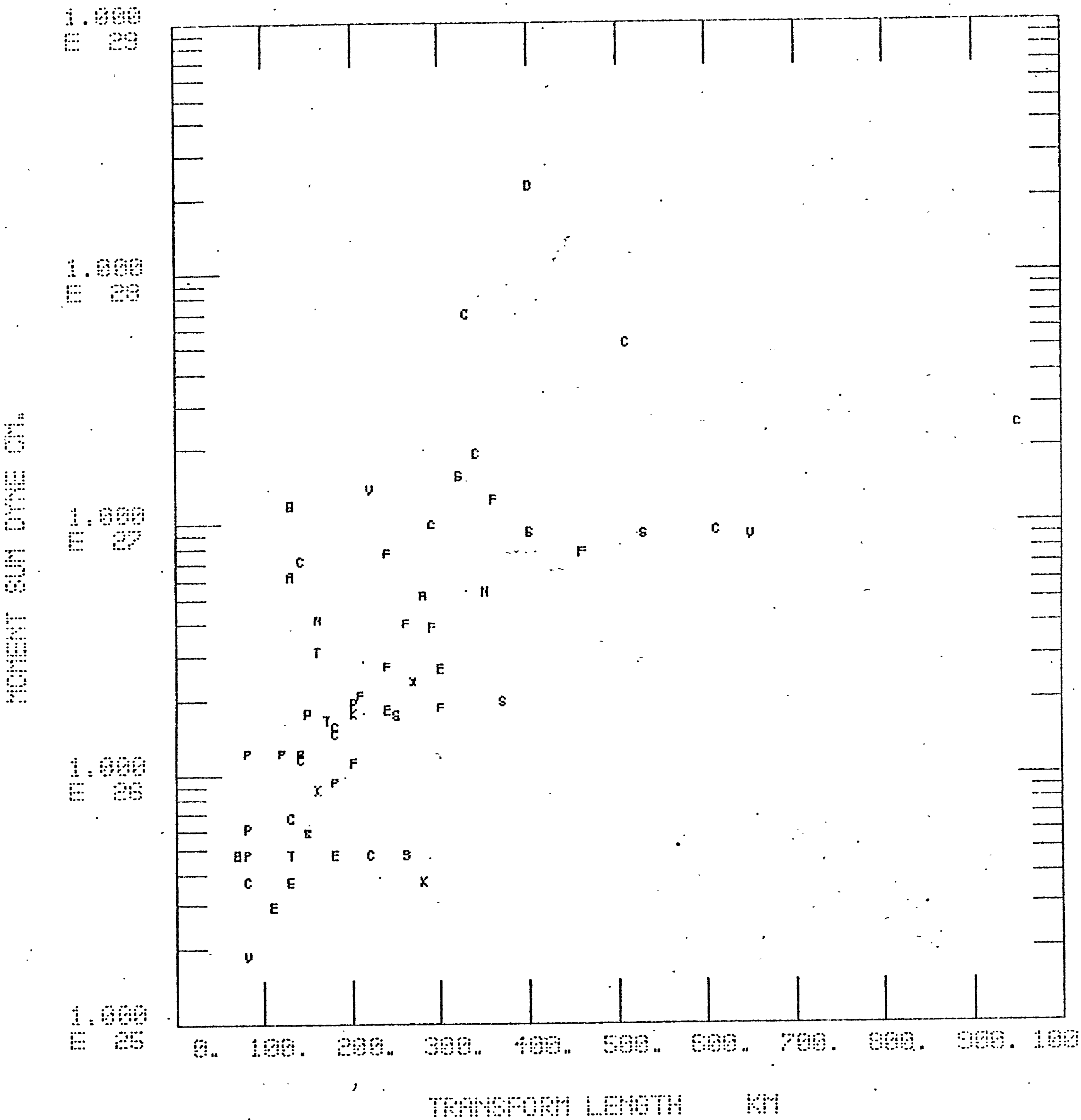

1.000 E 29
1.000 E 28
1.000 E 27
1.000 E 26
1.000 E 25
MOMENT SUM DYNE CM.
0.
100.
200.
300.
400.
500.
600.
700.
800.
900.
1000
TRANSFORM LENGTH KM


Figure 8

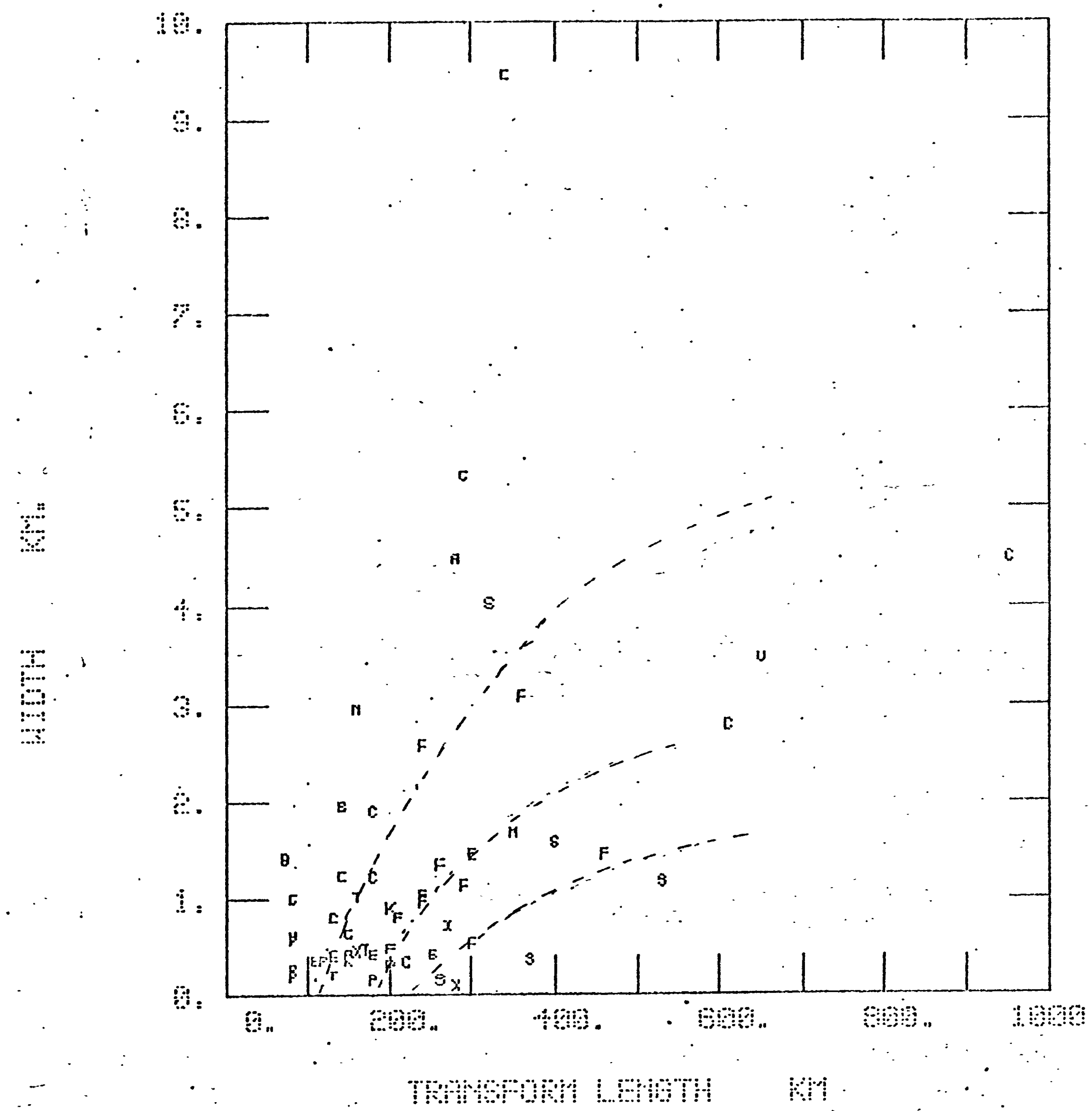
10.
9.
8.
7.
6.
5.
4.
3.
2.
1.
0.
WIDTH KM.
0.
200.
400.
600.
800.
1000.
TRANSFORM LENGTH KM

Figure 9

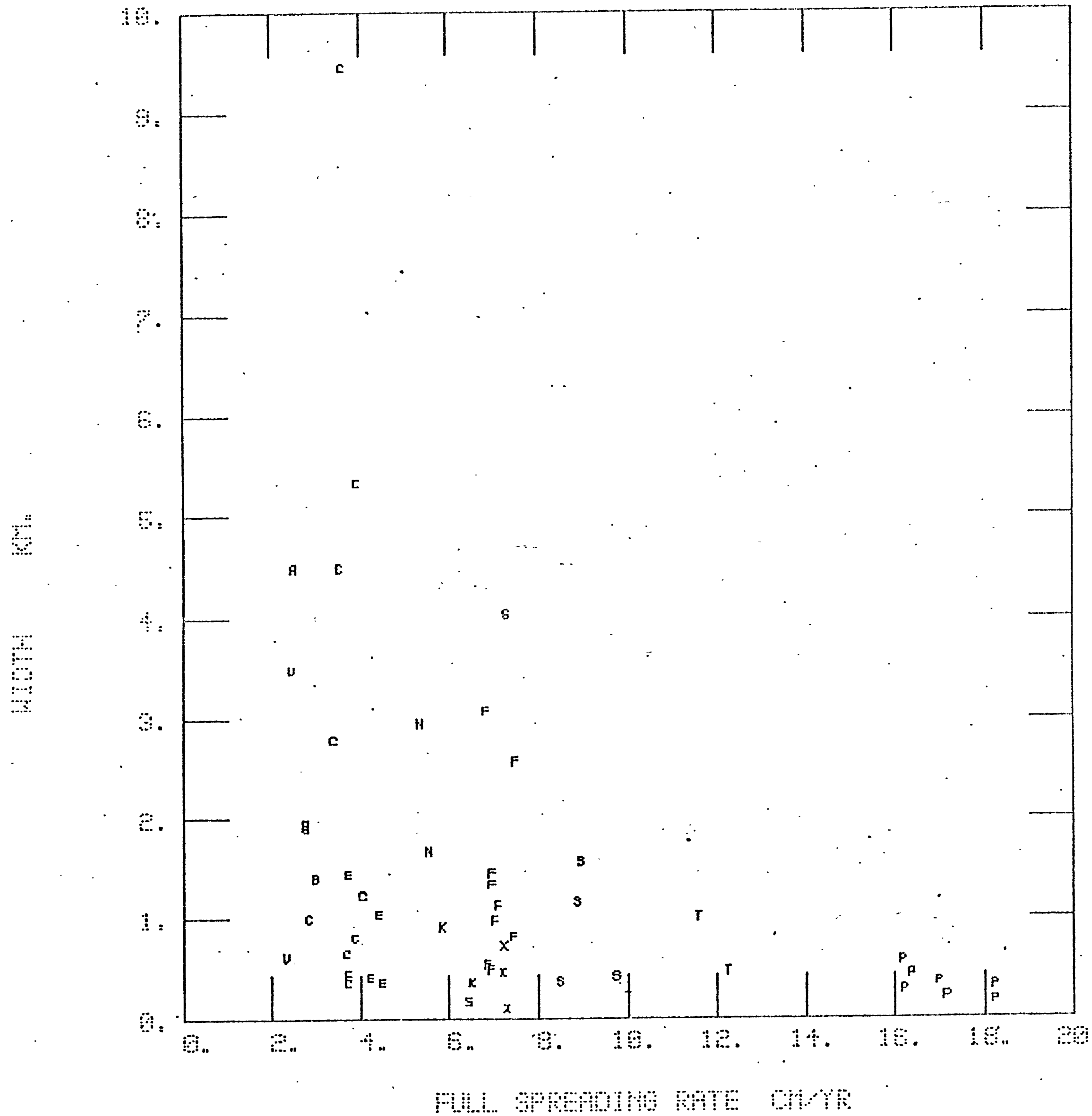

WIDTH KM.
FULL SPREADING RATE CM/YR
0.
2.
4.
6.
8.
10.
12.
14.
16.
18.
20.
1.
3.
5.
7.
9.


Figure 10

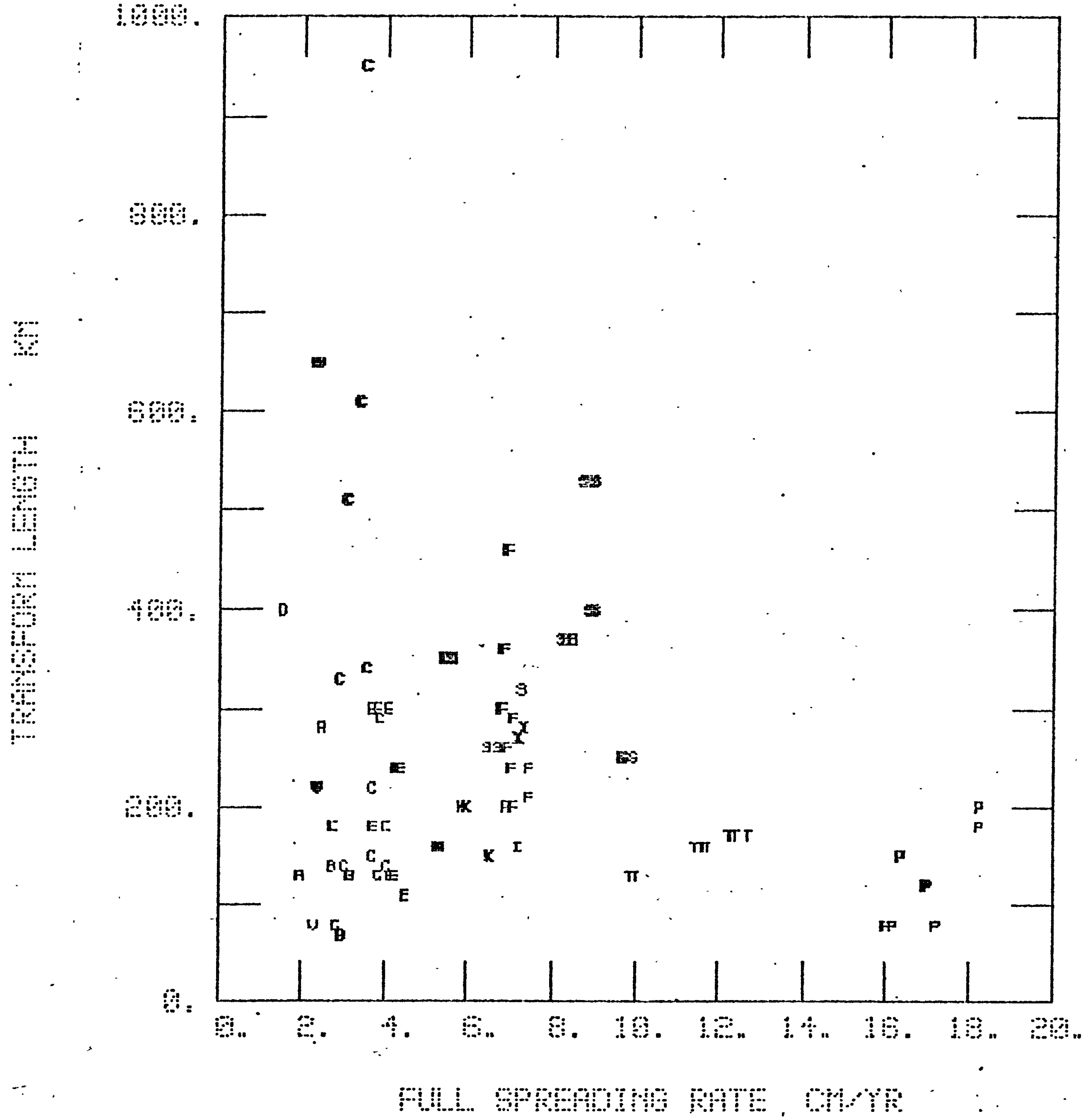

1000.
800.
600.
400.
200.
0.
0.
2.
4.
6.
8.
10.
12.
14.
16.
18.
20.
TRANSFORM LENGTH KM
FULL SPREADING RATE, CM/YR


Figure 11

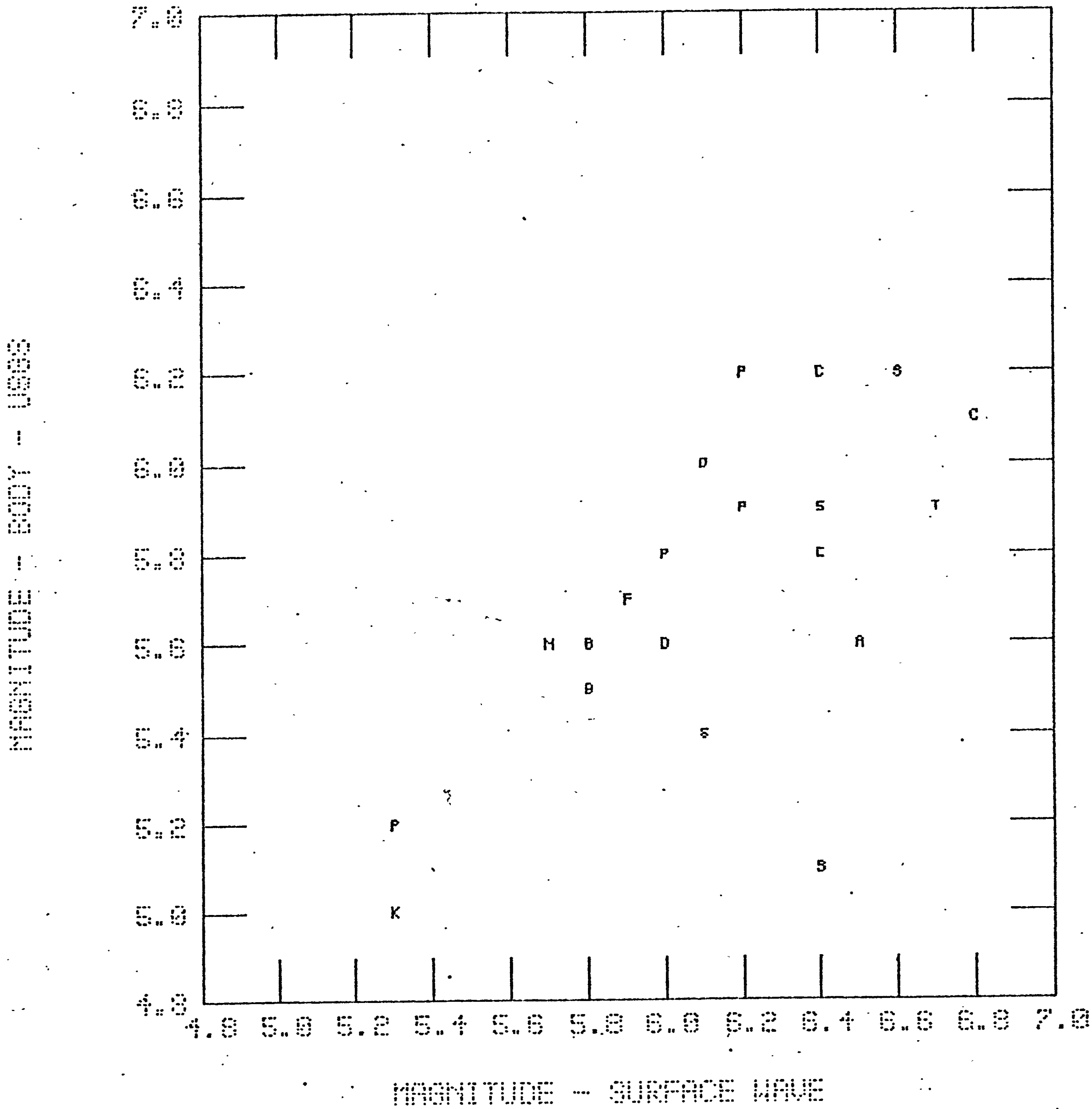
MAGNITUDE - BODY - USGS
MAGNITUDE - SURFACE WAVE
7.0
6.8
6.6
6.4
6.2
6.0
5.8
5.6
5.4
5.2
5.0
4.8
4.8 5.0 5.2 5.4 5.6 5.8 6.0 6.2 6.4 6.6 6.8 7.0

Figure 12

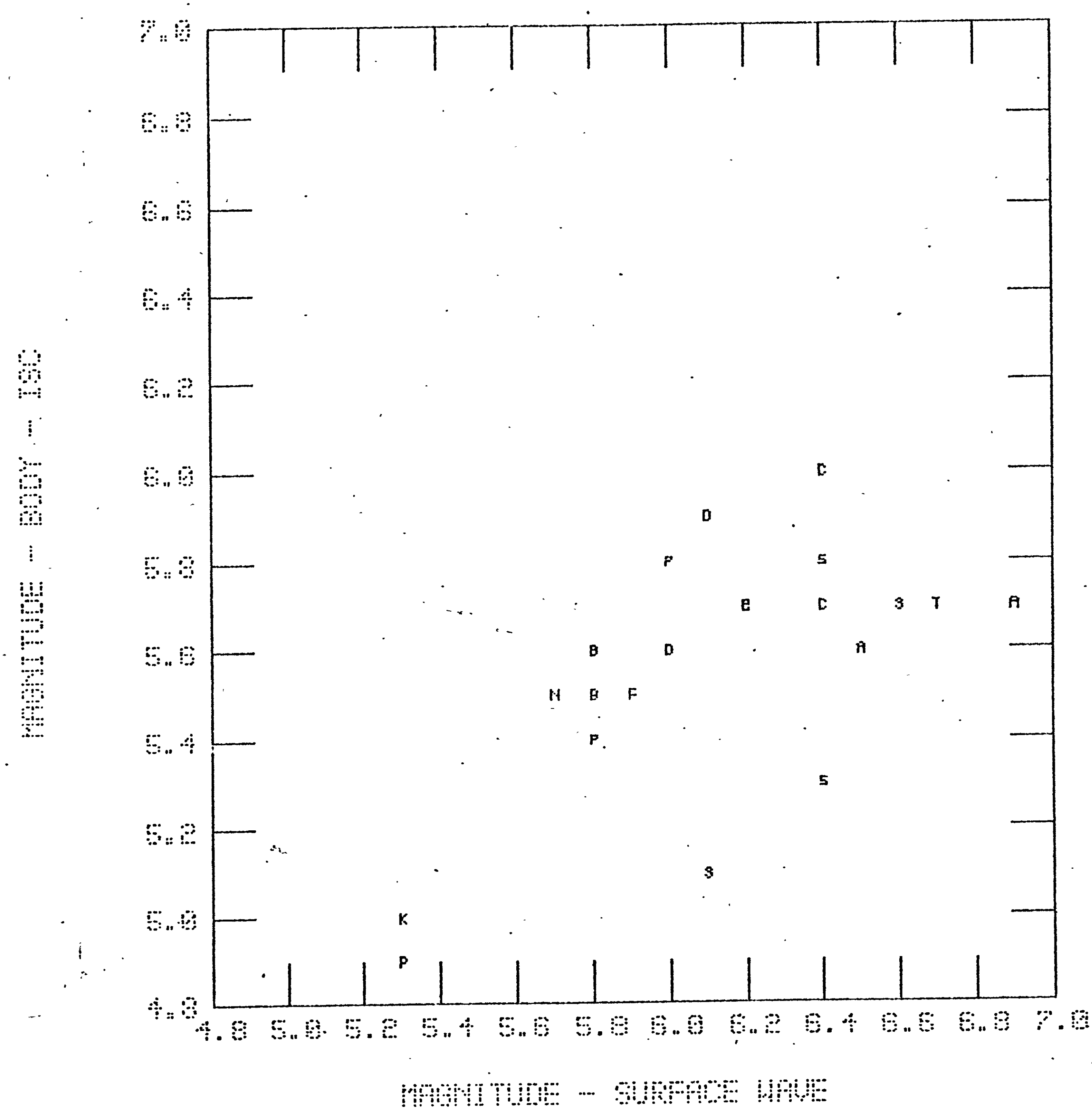
MAGNITUDE - BODY - ISC
MAGNITUDE - SURFACE WAVE
7.0
6.8
6.6
6.4
6.2
6.0
5.8
5.6
5.4
5.2
5.0
4.8
4.8 5.0 5.2 5.4 5.6 5.8 6.0 6.2 6.4 6.6 6.8 7.0

Figure 13

# BOUNDS ON FAULT AREA

V=10 cm/yr Full Spreading Rate

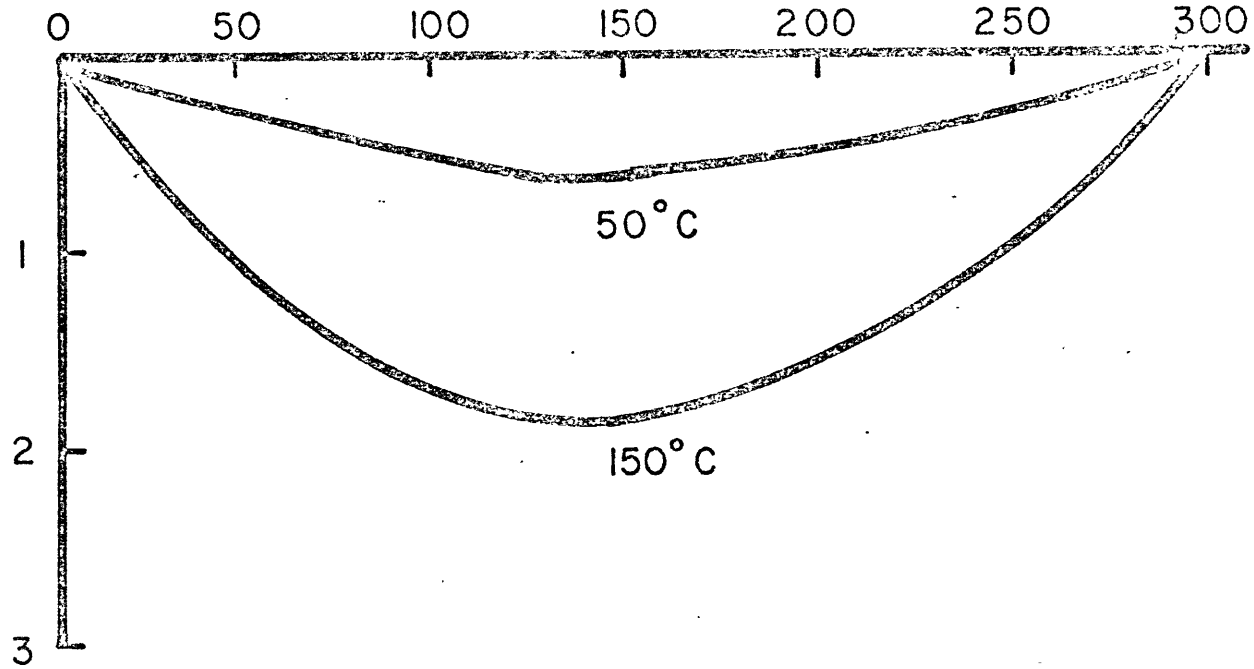


Figure 14a

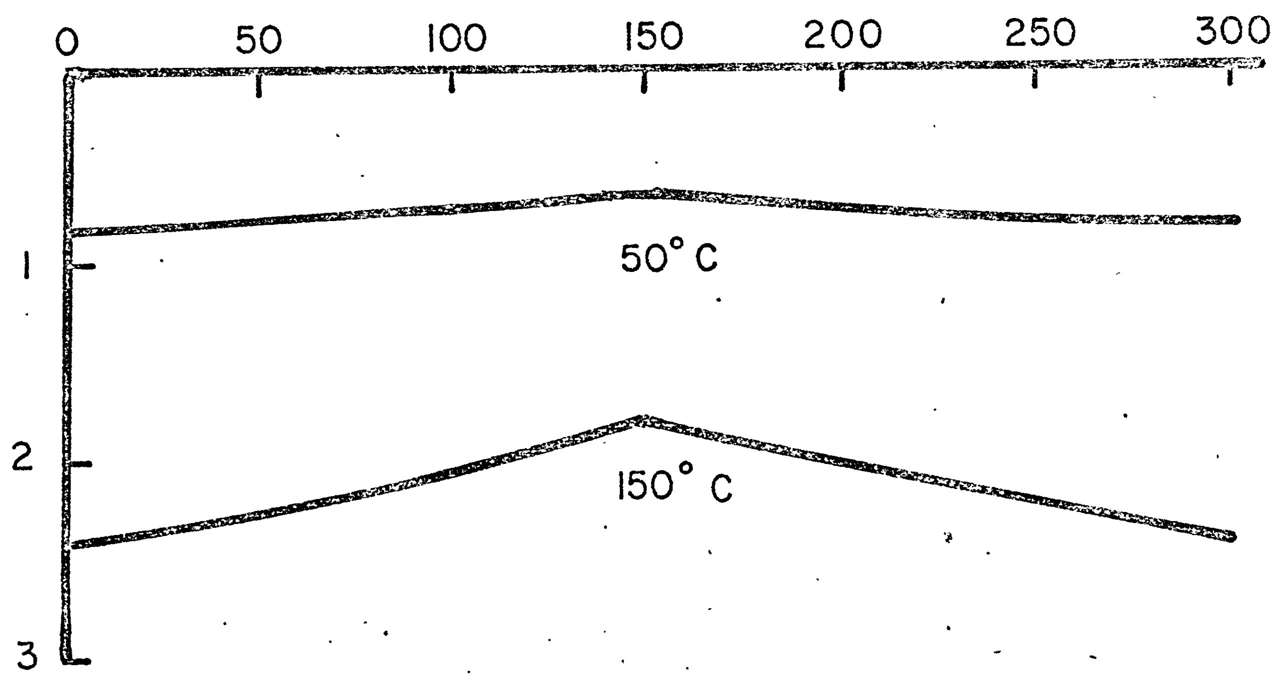


Figure 14b

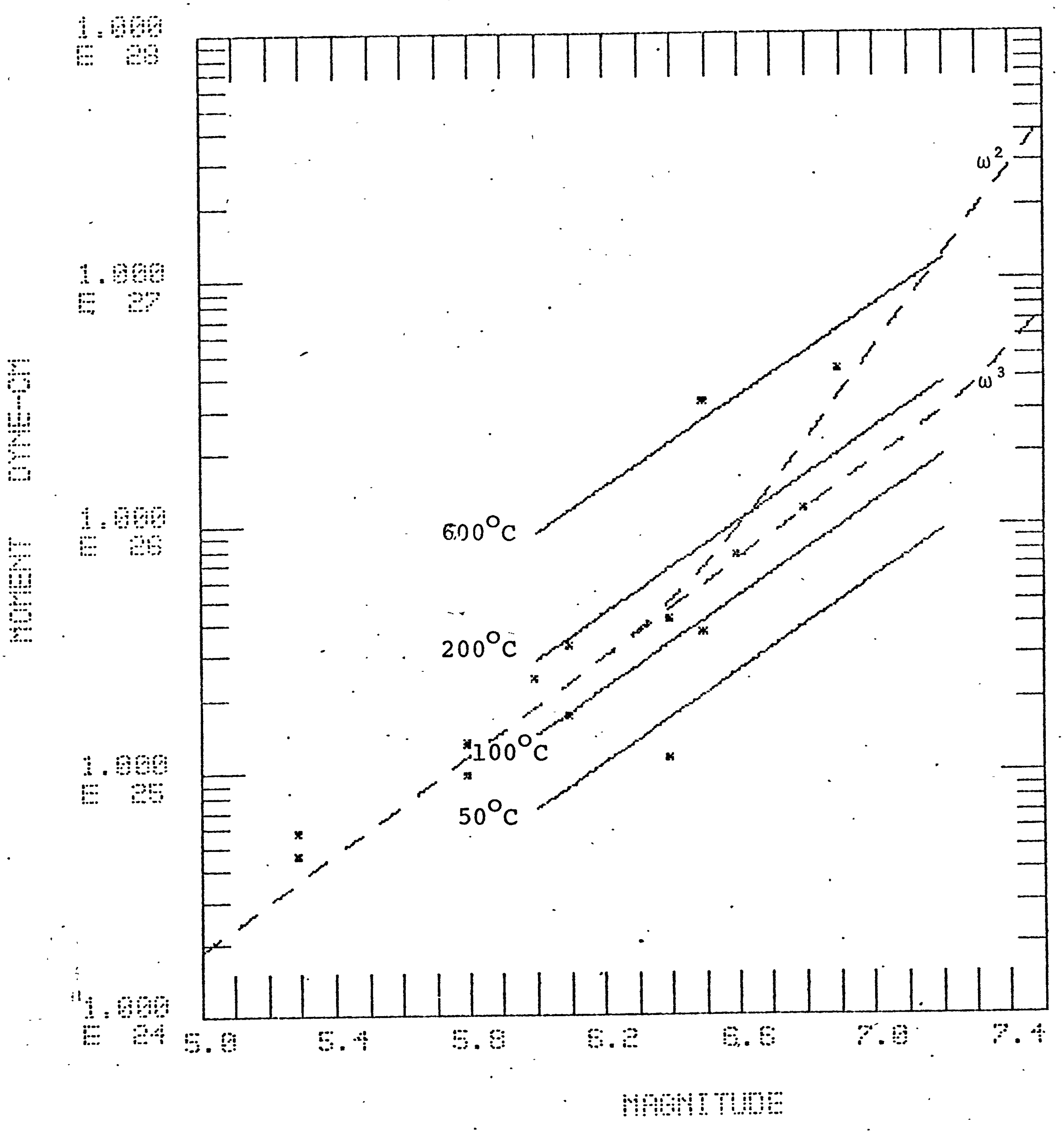

1.000 E 28
1.000 E 27
1.000 E 26
1.000 E 25
1.000 E 24
MOMENT DYNE-CM
5.0
5.4
5.8
6.2
6.6
7.0
7.4
MAGNITUDE
600°C
200°C
100°C
50°C
ω²
ω³


Figure 15

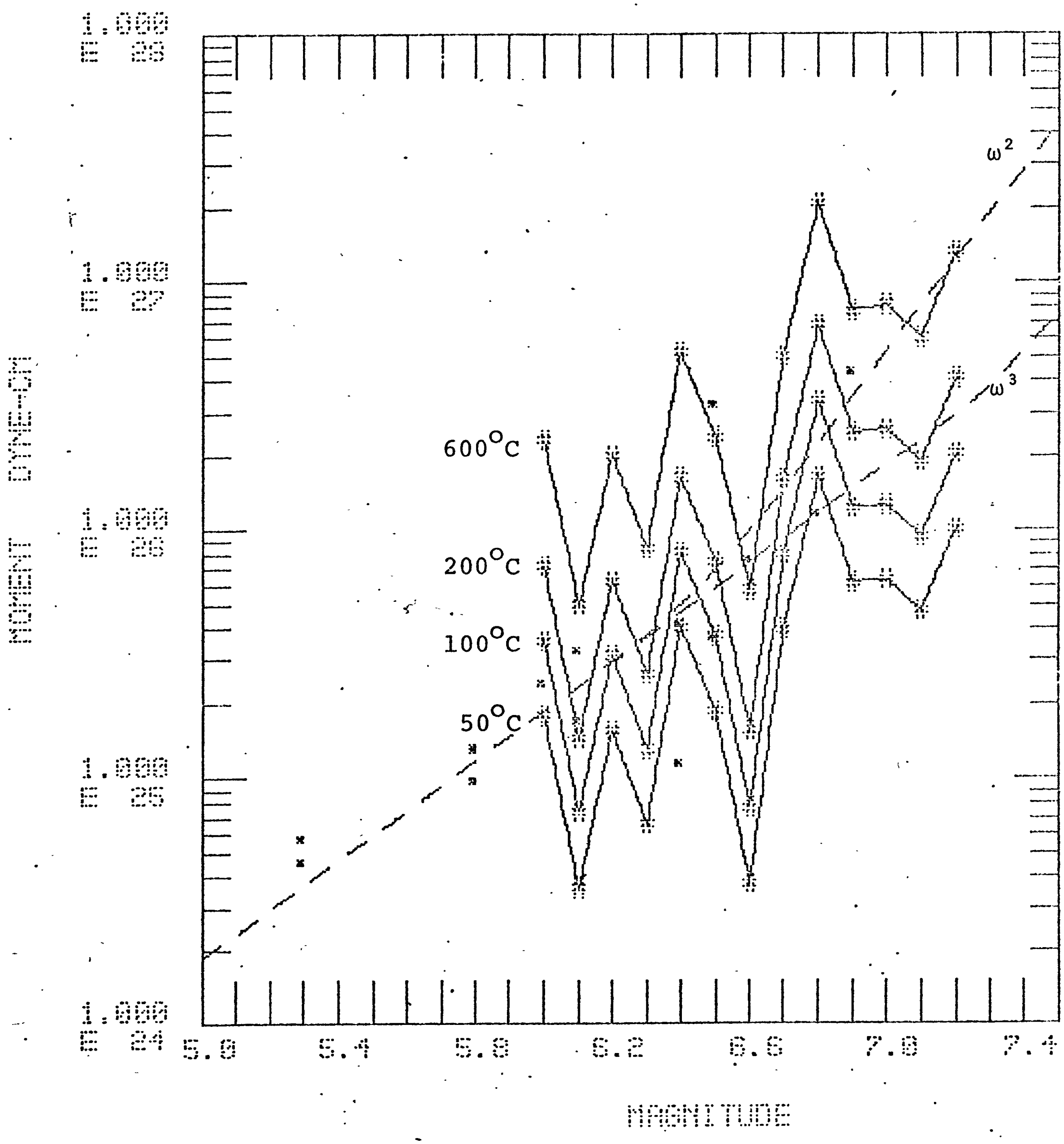
1.000 E 28
1.000 E 27
1.000 E 26
1.000 E 25
1.000 E 24
MOMENT DYNE-CM
5.0
5.4
5.8
6.2
6.6
7.0
7.4
MAGNITUDE
600°C
200°C
100°C
50°C
ω²
ω³

Figure 16

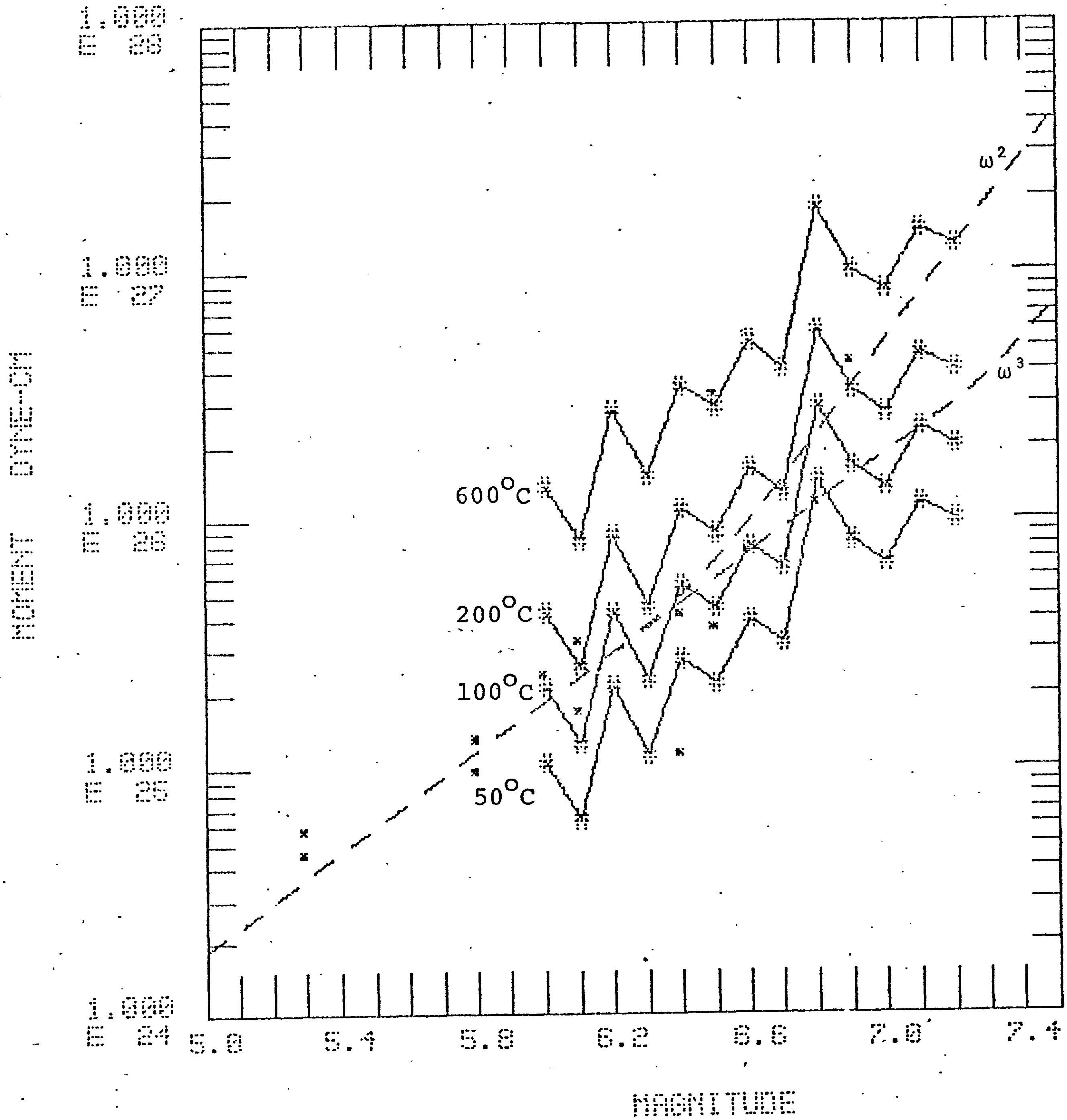
1.000
E 28
1.000
E 27
1.000
E 26
1.000
E 25
1.000
E 24
MOMENT DYNE-CM
5.0
5.4
5.8
6.2
6.6
7.0
7.4
MAGNITUDE
600°C
200°C
100°C
50°C
ω²
ω³

Figure 17

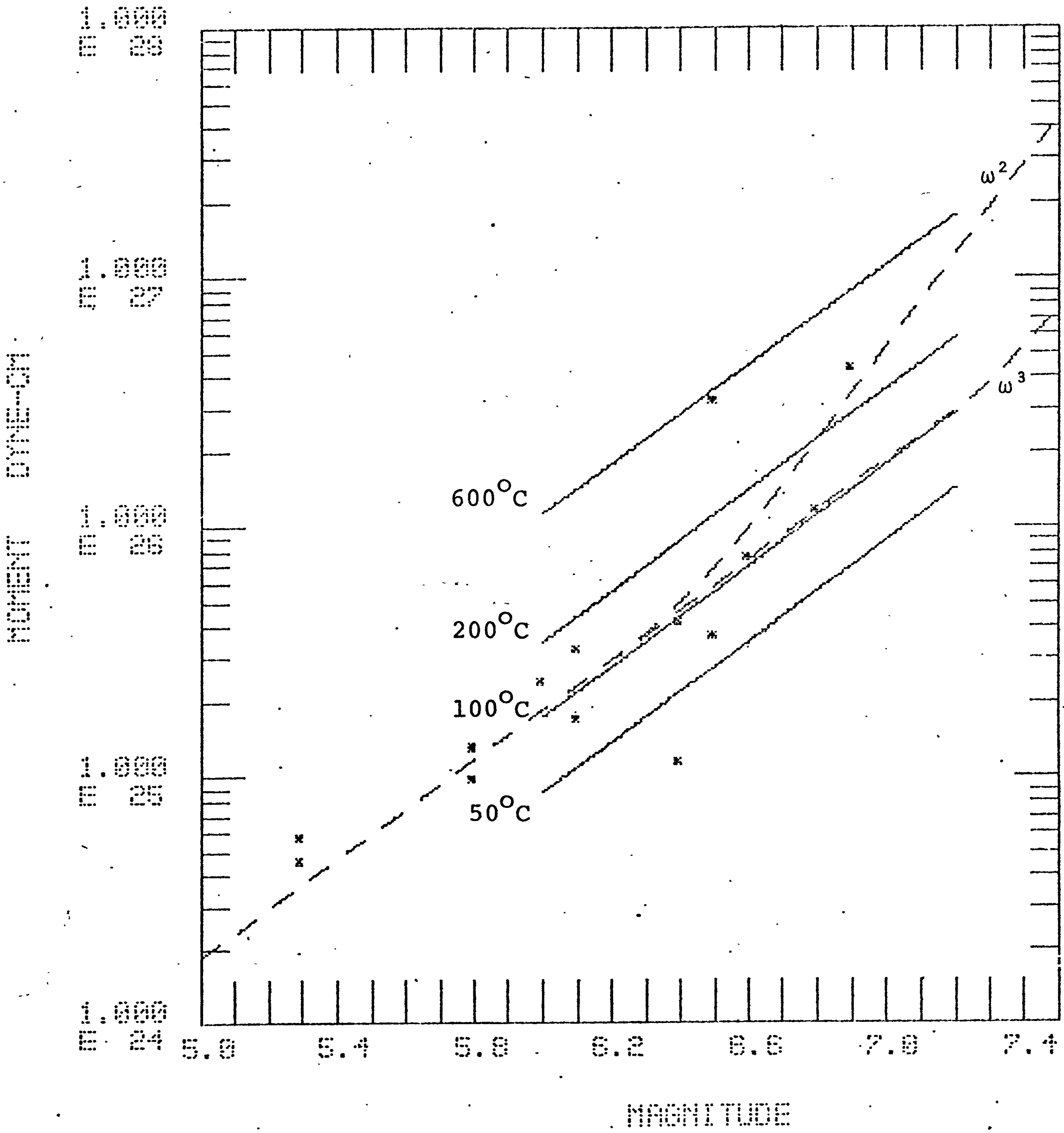

1.000 E 28
1.000 E 27
1.000 E 26
1.000 E 25
1.000 E 24
MOMENT DYNE-CM
5.0
5.4
5.8
6.2
6.6
7.0
7.4
MAGNITUDE
600°C
200°C
100°C
50°C
$\omega^2$
$\omega^3$


Figure 18

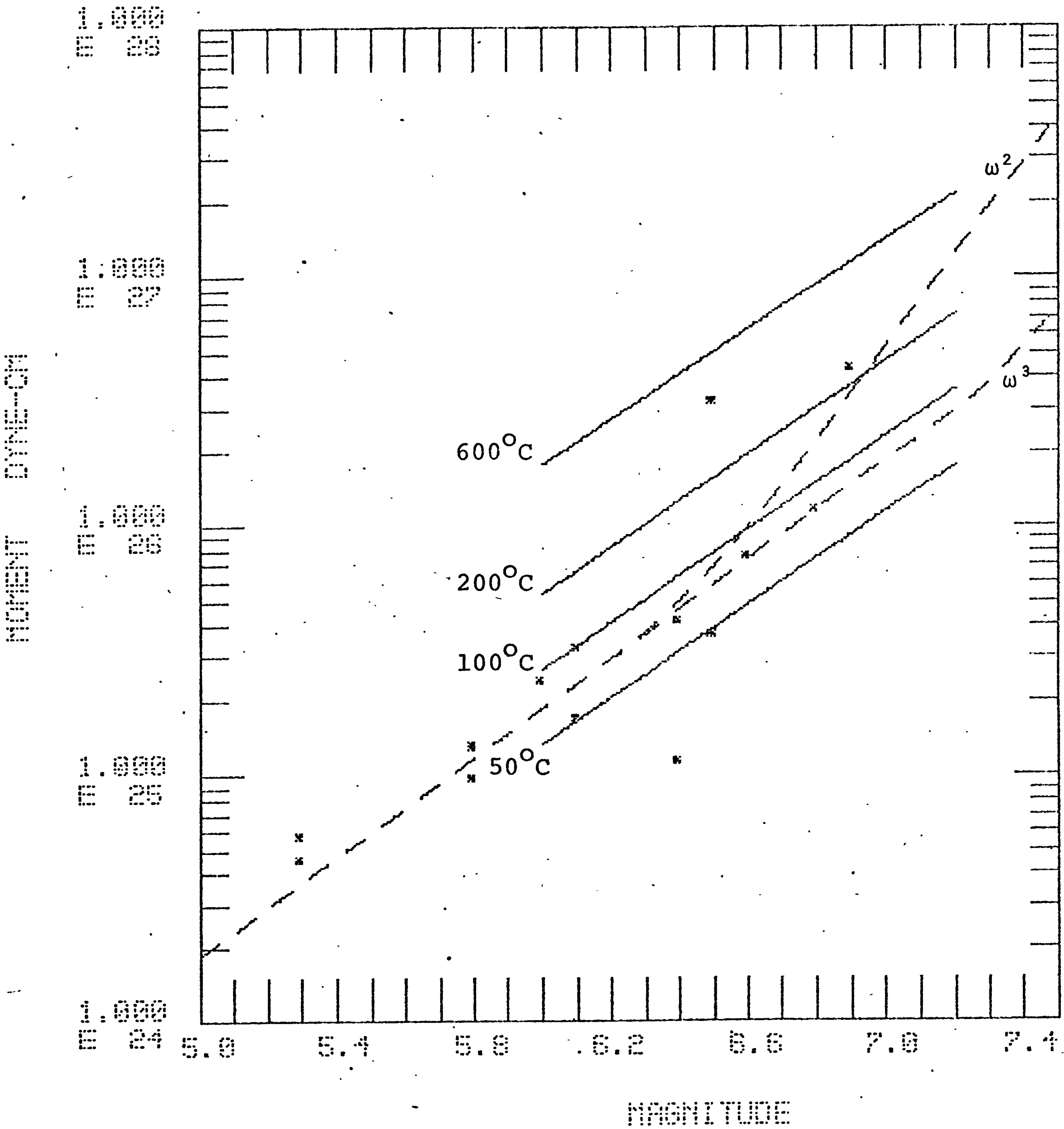
1.000 E 28
1.000 E 27
1.000 E 26
1.000 E 25
1.000 E 24
MOMENT DYNE-CM
5.0
5.4
5.8
6.2
6.6
7.0
7.4
MAGNITUDE
600°C
200°C
100°C
50°C
$\omega^2$
$\omega^3$

Figure 19

ROMANCHE TRANSFORM

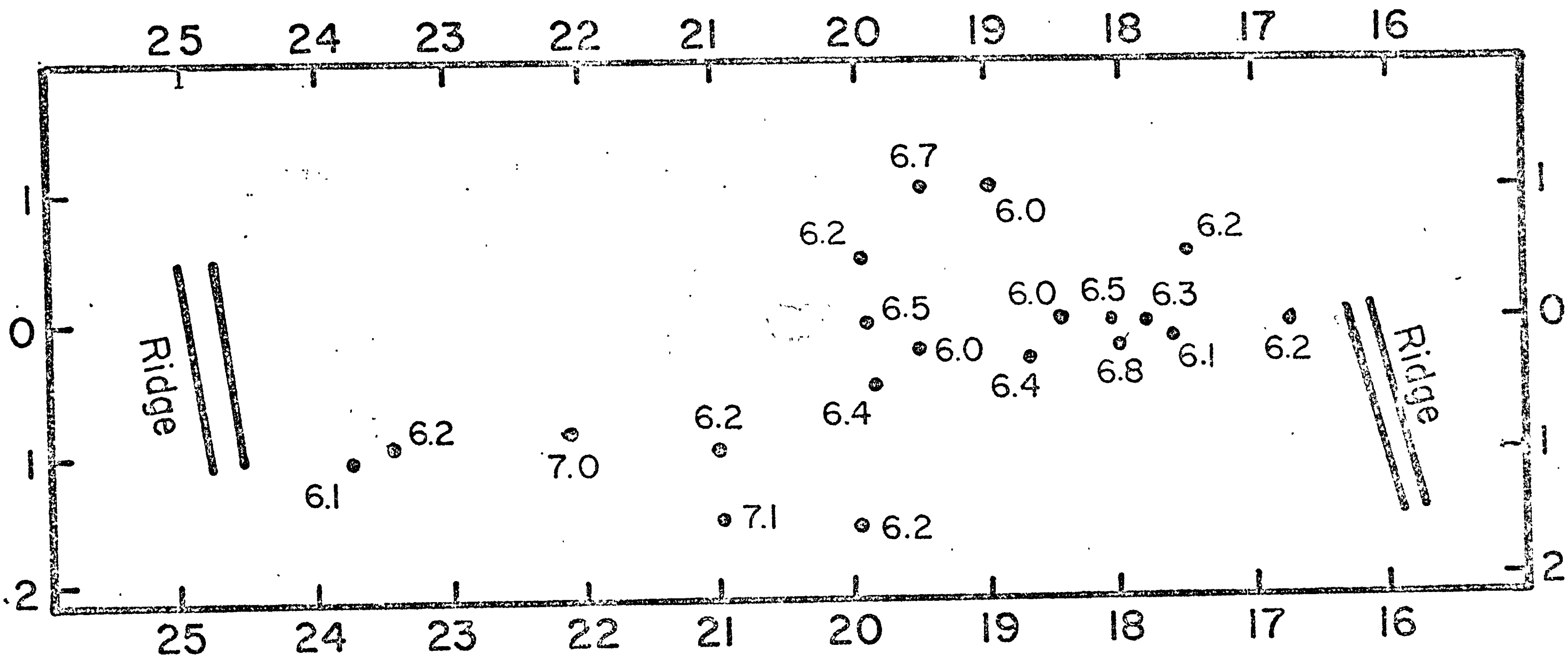


Figure 20

## APPENDIX 1

On the following pages the dates, locations, and magnitudes of all the earthquakes used in this study have been compiled. The first number represents the plate boundary (Table IV) where the earthquake is located and the second number is the arbitrary number assigned to the transform (as in Table I) where the earthquake occurs.

| | | | | | |
|---|---|---|---|---|---|
| 1 | 1 | 16 OCT 1974 | 52,636N | 32,270W | 6,9 |
| 1 | 1 | 13 FEB 1967 | 52,761N | 34,098W | 6,5 |
| 1 | 1 | 18 JUN 1941 | 52,000N | 34,500W | 6,2 |
| 1 | 1 | 11 DEC 1954 | 52,500N | 32,000W | 6,5 |
| 1 | 2 | 2 JUN 1934 | 66,000N | 18,250W | 6,2 |
| 1 | 2 | 23 AUG 1921 | 67,000N | 18,000W | 6,2 |
| 1 | 2 | 28 MAR 1963 | 66,300N | 19,400W | 7,0 |
| 2 | 1 | 19 MAY 1963 | 23,800N | 46,000W | 6,4 |
| 2 | 1 | 23 MAY 1935 | 23,000N | 45,000W | 6,2 |
| 2 | 1 | 12 AUG 1925 | 24,000N | 46,000W | 6,5 |
| 2 | 1 | 14 OCT 1924 | 24,000N | 45,000W | 6,5 |
| 2 | 1 | 9 JAN 1922 | 24,000N | 46,000W | 7,1 |
| 2 | 2 | 9 JUL 1953 | 30,200N | 42,200W | 6,2 |
| 2 | 2 | 6 FEB 1935 | 30,500N | 42,000W | 6,3 |
| 2 | 3 | 18 NOV 1970 | 35,147N | 35,736W | 6,0 |
| 2 | 3 | 19 MAR 1959 | 35,150N | 36,120W | 6,2 |
| 2 | 3 | 4 DEC 1932 | 35,500N | 36,500W | 6,3 |
| 2 | 3 | 23 DEC 1957 | 35,200N | 35,800W | 6,0 |
| 2 | 3 | 17 MAT 1964 | 35,200N | 35,900W | 6,3 |

| | | | | | |
|---|---|---|---|---|---|
| 3 | 1 | 26 NOV 197Ø | 43,776N | 127,449W | 6,Ø |
| 3 | 1 | 8 MAY 1968 | 43,567N | 127,899W | 6,3 |
| 3 | 1 | 24 SEP 1964 | 43,5ØØN | 127,5ØØW | 6,Ø |
| 3 | 1 | 1 OCT 1964 | 43,5ØØN | 126,ØØØW | 6,2 |
| 3 | 1 | 26 SEP 1959 | 43,5ØØN | 128,5ØØW | 6,1 |
| 3 | 1 | 23 AUG 1955 | 43,5ØØN | 128,ØØØW | 6,2 |
| 3 | 1 | 2Ø AUG 1952 | 43,25ØN | 126,5ØØW | 6,5 |
| 3 | 1 | 17 JUN 1951 | 44,5ØØN | 13Ø,ØØØW | 6,3 |
| 3 | 1 | 28 MAY 1938 | 42,75ØN | 126,ØØØW | 6,Ø |
| 3 | 1 | 11 SEP 1928 | 43,5ØØN | 13Ø,25ØW | 6,3 |
| 3 | 1 | 5 JUN 1926 | 43,ØØØN | 127,5ØØW | 6,Ø |
| 3 | 1 | 1Ø JUN 1917 | 44,ØØØN | 129,ØØØW | 6,5 |
| 3 | 1 | 22 AUG 1914 | 44,ØØØN | 129,ØØØW | 6,7 |
| 3 | 2 | 5 DEC 1971 | 49,625N | 129,45ØW | 6,3 |
| 3 | 2 | 1 DEC 196Ø | 49,ØØØN | 129,3ØØW | 6,Ø |
| 3 | 2 | 28 JUN 1956 | 48,75ØN | 129,25ØW | 6,3 |
| 3 | 2 | 4 DEC 1953 | 49,5ØØN | 129,ØØØW | 6,2 |
| 3 | 2 | 18 JUL 1939 | 49,ØØØN | 129,25ØW | 6,5 |
| 3 | 2 | 24 SEP 1935 | 49,5ØØN | 13Ø,ØØØW | 6,2 |
| 3 | 2 | 1 NOV 1926 | 48,75ØN | 128,5ØØW | 6,6 |
| 3 | 2 | 3Ø OCT 1926 | 48,5ØØN | 129,ØØØW | 6,1 |
| 3 | 2 | 3Ø MAR 1924 | 5Ø,ØØØN | 13Ø,25ØW | 6,Ø |
| 3 | 2 | 21 JUL 1914 | 49,ØØØN | 13Ø,ØØØW | 6,5 |

| | | | | | |
|---|---|---|---|---|---|
| 4 | 1 | 24 JUN 1934 | 2,500S | 106,500W | 6,0 |
| 4 | 1 | 14 OCT 1955 | 3,000S | 103,500W | 6,1 |
| 4 | 1 | 20 FEB 1934 | 4,000S | 105,000W | 6,0 |
| 4 | 2 | 21 SEP 1973 | 4,387S | 102,003W | 6,2 |
| 4 | 2 | 21 SEP 1973 | 4,364S | 101,939W | 6,1 |
| 4 | 2 | 10 MAY 1974 | 4,372S | 102,109W | 6,5 |
| 4 | 3 | 16 SEP 1950 | 4,600S | 105,100W | 6,5 |
| 4 | 3 | 18 APR 1950 | 4,500S | 106,000W | 6,5 |
| 4 | 3 | 10 APR 1958 | 4,500S | 107,000W | 6,0 |
| 4 | 3 | 12 JUL 1958 | 5,000S | 106,500W | 6,0 |
| 4 | 4 | 5 MAR 1936 | 9,500S | 108,000W | 6,0 |
| 4 | 4 | 23 JUL 1939 | 9,000S | 109,000W | 6,0 |
| 4 | 4 | 14 JAN 1948 | 9,000S | 109,000W | 6,2 |
| 4 | 4 | 28 APR 1955 | 9,000S | 108,200W | 6,0 |
| 4 | 4 | 12 JUN 1956 | 9,000S | 110,000W | 6,3 |
| 4 | 5 | 5 AUG 1944 | 13,500S | 92,500W | 6,0 |
| 4 | 5 | 5 AUG 1944 | 13,500S | 92,500W | 6,2 |
| 4 | 6 | 18 JUL 1912 | 28,000S | 114,000W | 6,5 |
| 4 | 6 | 25 JUN 1926 | 28,000S | 115,000W | 6,2 |
| 4 | 6 | 2 JAN 1940 | 28,500S | 113,000W | 6,2 |
| 4 | 6 | 19 SEP 1943 | 28,000S | 113,000W | 6,2 |
| 4 | 6 | 22 APR 1944 | 28,000S | 113,500W | 6,0 |
| 4 | 6 | 18 NOV 1944 | 28,000S | 112,000W | 6,0 |
| 4 | 7 | 21 AUG 1962 | 29,600S | 111,900W | 6,3 |
| 4 | 7 | 17 FEB 1960 | 30,000S | 112,500W | 6,3 |
| 4 | 7 | 16 JUL 1958 | 29,500S | 113,000W | 6,0 |

| | | | | | |
|---|---|---|---|---|---|
| 5 | 1 | 6 FEB 1957 | 1,81ØN | 92,56ØW | 6,Ø |
| 5 | 1 | 5 MAY 1926 | 3,ØØØN | 91,ØØØW | 6,5 |
| 5 | 1 | 4 FEB 1938 | 3,ØØØN | 91,ØØØW | 6,[illegible] |
| 5 | 1 | 4 JUN 1954 | Ø,7[illegible]ØS | 91,7ØØW | 6,5 |
| | | | | | |
| 5 | 2 | 23 NOV 1935 | Ø,5ØØN | 85,5ØØW | 6,2 |
| 5 | 2 | 5 APR 1969 | 1,2[illegible]1N | 85,212W | 6,2 |
| | | | | | |
| 6 | 1 | 8 APR 1964 | 6,8ØØS | 68,9ØØE | 6,2 |
| 6 | 1 | 16 JUL 1932 | 7,ØØØS | 68,ØØØE | 6,Ø |
| | | | | | |
| 6 | 2 | 11 MAY 1912 | 9,ØØØS | 72,ØØØE | 6,8 |
| 6 | 2 | 10 MAY 1963 | 8,2[illegible]ØS | 68,1ØØE | 6,2 |
| 6 | 2 | 3 JUL 1922 | 8,5ØØS | 66,ØØØE | 6,[illegible] |
| | | | | | |
| 6 | 3 | 14 FEB 1922 | 13,5ØØS | 67,ØØØE | 6,[illegible] |
| 6 | 3 | 10 DEC 1944 | 14,ØØØS | 68,5ØØE | 6,[illegible] |
| | | | | | |
| 6 | 4 | 19 MAY 1960 | 17,ØØØS | 66,ØØØE | 6,[illegible] |
| 6 | 4 | 31 DEC 1931 | 17,ØØØS | 64,ØØØE | 6,2 |
| 6 | 4 | 18 MAR 1932 | 17,ØØØS | 65,5ØØE | 6,[illegible] |
| 6 | 4 | 21 MAR 1936 | 17,ØØØS | 66,ØØØE | 6,2 |
| 6 | 4 | 30 JUN 1941 | 17,ØØØS | 65,ØØØE | 6,[illegible] |
| 6 | 4 | 4 FEB 1955 | 17,2[illegible]ØS | 66,8ØØE | 6,3 |
| 6 | 4 | 3 JUL 1958 | 18,ØØØS | 66,ØØØE | 6,2 |
| | | | | | |
| 6 | 5 | 14 FEB 1932 | 19,ØØØS | 66,5ØØE | 6,2 |

| | | | | | |
|---|---|---|---|---|---|
| 7 | 1 | 9 APR 1959 | 36,300S | 76,800E | 6,0 |
| 7 | 1 | 10 JUL 1968 | 36,806S | 78,542E | 6,1 |
| 7 | 1 | 20 FEB 1940 | 37,500S | 79,000E | 6,5 |
| 7 | 1 | 11 JUL 1959 | 37,000S | 79,000E | 6,3 |
| 7 | 1 | 5 OCT 1929 | 37,000S | 78,000E | 6,0 |
| 7 | 1 | 7 MAR 1961 | 38,400S | 78,100E | 6,0 |
| 7 | 2 | 21 OCT 1954 | 41,000S | 80,500E | 6,7 |
| 7 | 2 | 31 MAY 1928 | 41,500S | 80,000E | 6,2 |
| 7 | 2 | 11 DEC 1924 | 41,000S | 80,000E | 6,2 |
| 7 | 2 | 18 APR 1945 | 42,000S | 80,000E | 6,5 |
| 7 | 3 | 22 OCT 1964 | 45,600S | 96,100E | 6,2 |
| 7 | 3 | 8 FEB 1973 | 45,475S | 96,288E | 6,1 |
| 7 | 3 | 6 APR 1966 | 45,800S | 96,200E | 6,0 |
| 7 | 3 | 7 MAY 1956 | 46,500S | 96,000E | 6,5 |
| 7 | 3 | 19 MAY 1956 | 41,600S | 42,200E | 0,0 |
| 7 | 3 | 1 MAR 1936 | 47,000S | 96,000E | 6,5 |
| 7 | 4 | 9 SEP 1957 | 48,000S | 94,700E | 6,0 |
| 7 | 4 | 1 JUN 1973 | 47,796S | 99,661E | 6,3 |
| 7 | 4 | 1 AUG 1942 | 48,000S | 99,000E | 7,0 |
| 7 | 4 | 8 MAY 1938 | 48,000S | 99,000E | 6,7 |
| 7 | 5 | 21 AUG 1959 | 50,500S | 139,600E | 6,1 |
| 7 | 5 | 5 DEC 1961 | 50,800S | 139,700E | 6,2 |
| 7 | 5 | 23 APR 1946 | 50,000S | 140,000E | 6,7 |
| 7 | 5 | 14 JUN 1927 | 50,000S | 140,000E | 6,5 |
| 7 | 5 | 24 AUG 1936 | 51,000S | 140,000E | 6,2 |
| 7 | 5 | 31 DEC 1927 | 51,000S | 140,000E | 6,0 |
| 7 | 5 | 7 JAN 1921 | 51,000S | 140,000E | 6,2 |
| 7 | 5 | 2 JUL 1970 | 51,035S | 139,487E | 6,1 |
| 7 | 5 | 31 DEC 1929 | 51,000S | 138,000E | 6,0 |
| 7 | 6 | 17 JAN 1958 | 51,600S | 139,800E | 6,0 |
| 7 | 6 | 4 FEB 1965 | 51,800S | 139,700E | 6,0 |
| 7 | 6 | 28 JUL 1964 | 51,200S | 139,000E | 6,3 |
| 7 | 6 | 25 DEC 1931 | 52,000S | 141,000E | 6,0 |
| 7 | 6 | 12 OCT 1937 | 53,000S | 145,000E | 6,0 |

| | | | | | |
|---|---|---|---|---|---|
| 7 | 7 | 20 JUL 1963 | 57,600S | 148,500E | 6,4 |
| 7 | 7 | 23 MAR 1955 | 56,200S | 147,500E | 6,0 |
| 7 | 7 | 27 APR 1954 | 56,100S | 147,300E | 6,0 |
| 7 | 7 | 10 JUN 1963 | 55,900S | 146,200E | 6,2 |
| 7 | 7 | 10 JUN 1963 | 55,200S | 146,100E | 6,4 |
| 7 | 7 | 17 DEC 1961 | 54,500S | 143,900E | 6,1 |
| 7 | 7 | 20 SEP 1952 | 54,900S | 144,600E | 6,3 |
| 7 | 7 | 25 SEP 1973 | 54,649S | 145,849E | 6,3 |
| 7 | 7 | 14 MAR 1940 | 56,000S | 145,000E | 6,7 |
| 7 | 7 | 26 APR 1925 | 56,000S | 147,000E | 6,2 |
| 7 | 7 | 7 SEP 1927 | 56,000S | 148,000E | 6,2 |
| 7 | 7 | 7 MAY 1950 | 56,900S | 148,500E | 6,4 |
| 7 | 7 | 17 DEC 1942 | 57,000S | 146,000E | 6,0 |
| 7 | 7 | 1 OCT 1958 | 57,090S | 147,650E | 6,2 |
| 7 | 7 | 8 AUG 1940 | 57,500S | 147,000E | 6,2 |
| 7 | 7 | 11 JUN 1950 | 57,500S | 148,000E | 6,3 |
| 7 | 7 | 29 MAR 1940 | 57,000S | 144,000E | 6,0 |
| 7 | 7 | 27 FEB 1933 | 57,500S | 144,000E | 6,0 |
| 7 | 7 | 1 DEC 1931 | 57,000S | 144,000E | 6,5 |
| 7 | 7 | 24 NOV 1934 | 57,000S | 146,000E | 6,2 |
| | | | | | |
| 7 | 8 | 27 APR 1944 | 60,100S | 151,000E | 6,2 |
| 7 | 8 | 13 OCT 1957 | 60,400S | 150,900E | 6,5 |
| 7 | 8 | 16 SEP 1952 | 59,250S | 147,250E | 6,0 |
| 7 | 8 | 29 FEB 1928 | 58,500S | 148,000E | 6,2 |
| 7 | 8 | 25 JUL 1952 | 59,300S | 148,800E | 6,5 |
| 7 | 8 | 14 AUG 1925 | 59,000S | 151,000E | 6,5 |
| 7 | 8 | 13 DEC 1930 | 60,000S | 150,000E | 6,0 |
| 7 | 8 | 14 SEP 1930 | 60,000S | 149,000E | 6,2 |
| 7 | 8 | 17 NOV 1940 | 61,000S | 148,000E | 6,5 |
| | | | | | |
| 7 | 9 | 1 DEC 1959 | 62,900S | 155,700E | 6,3 |
| 7 | 9 | 25 OCT 1962 | 61,400S | 154,900E | 6,0 |
| 7 | 9 | 22 MAR 1960 | 61,500S | 154,000E | 6,4 |
| 7 | 9 | 11 NOV 1965 | 60,600S | 153,700E | 6,1 |
| 7 | 9 | 31 MAY 1952 | 60,500S | 153,200E | 6,3 |
| 7 | 9 | 23 MAR 1945 | 62,000S | 153,000E | 7,1 |
| 7 | 9 | 1 DEC 1931 | 63,000S | 153,000E | 6,2 |
| 7 | 9 | 22 MAY 1929 | 62,000S | 155,000E | 6,5 |

| | | | | | |
|---|---|---|---|---|---|
| 9 | 1 | 29 DEC 1944 | 8,000N | 104,000W | 6,3 |
| 9 | 1 | 29 DEC 1944 | 8,500N | 104,000W | 6,2 |
| 9 | 1 | 21 JAN 1970 | 7,017N | 104,298W | 6,6 |
| 9 | 1 | 20 JAN 1954 | 8,500N | 103,500W | 6,3 |
| 9 | 2 | 28 MAY 1936 | 10,500N | 103,500W | 6,7 |
| 9 | 2 | 1 OCT 1976 | 11,000N | 104,000W | 6,7 |
| 9 | 2 | 15 JUL 1948 | 10,500N | 104,000W | 6,7 |
| 9 | 2 | 10 JAN 1950 | 10,000N | 104,000W | 6,2 |
| 9 | 2 | 16 AUG 1967 | 10,500N | 104,000W | 6,6 |
| 9 | 3 | 20 JAN 1955 | 15,500N | 104,400W | 6,2 |
| 9 | 3 | 25 JAN 1931 | 15,000N | 105,000W | 6,0 |

| | | | | | |
|---|---|---|---|---|---|
| 10 | 1 | 19 APR 1933 | 51,000S | 116,000W | 6,0 |
| 10 | 1 | 27 OCT 1934 | 48,000S | 116,000W | 6,2 |
| 10 | 1 | 5 JUN 1956 | 51,000S | 112,500W | 6,3 |
| 10 | 1 | 4 NOV 1958 | 50,000S | 115,000W | 6,0 |
| 10 | 1 | 2 AUG 1951 | 50,000S | 115,000W | 6,5 |
| 10 | 2 | 2 MAY 1957 | 55,900S | 123,500W | 6,5 |
| 10 | 2 | 3 JUL 1958 | 56,000S | 124,300W | 6,0 |
| 10 | 2 | 3 SEP 1944 | 57,000S | 122,000W | 7,0 |
| 10 | 2 | 19 OCT 1956 | 55,860S | 122,460W | 6,5 |
| 10 | 2 | 16 MAY 1935 | 55,000S | 123,000W | 6,2 |
| 10 | 2 | 16 FEB 1929 | 56,000S | 121,000W | 6,2 |
| 10 | 2 | 18 AUG 1969 | 56,022S | 123,367W | 6,4 |
| 10 | 2 | 4 APR 1971 | 56,245S | 122,459W | 6,6 |
| 10 | 3 | 3 APR 1963 | 55,500S | 128,100W | 6,5 |
| 10 | 3 | 22 NOV 1959 | 54,600S | 136,000W | 6,0 |
| 10 | 3 | 23 JAN 1951 | 55,000S | 136,500W | 6,8 |
| 10 | 3 | 10 MAR 1932 | 55,000S | 135,000W | 6,5 |
| 10 | 3 | 14 FEB 1941 | 53,500S | 131,000W | 6,5 |
| 10 | 3 | 13 NOV 1943 | 55,000S | 129,000W | 6,5 |
| 10 | 3 | 6 JAN 1930 | 55,000S | 131,000W | 6,0 |
| 10 | 3 | 20 JAN 1940 | 55,000S | 133,000W | 6,7 |
| 10 | 3 | 13 AUG 1937 | 56,500S | 130,000W | 6,0 |
| 10 | 3 | 1 APR 1944 | 57,000S | 128,000W | 6,0 |
| 10 | 3 | 20 MAY 1953 | 53,200S | 134,000W | 6,2 |
| 10 | 3 | 13 MAR 1966 | 55,500S | 126,500W | 6,2 |
| 10 | 3 | 9 SEP 1967 | 54,800S | 136,000W | 6,1 |
| 10 | 3 | 26 MAR 1971 | 55,439S | 129,100W | 6,0 |
| 10 | 3 | 7 MAY 1972 | 53,713S | 134,214W | 6,3 |
| 10 | 3 | 7 AUG 1973 | 54,351S | 136,550W | 6,1 |
| 10 | 3 | 18 SEP 1973 | 54,518S | 132,624W | 6,3 |
| 10 | 4 | 3 JUL 1952 | 56,300S | 142,500W | 6,2 |
| 10 | 4 | 7 NOV 1957 | 57,500S | 143,500W | 6,0 |
| 10 | 4 | 24 AUG 1970 | 56,600S | 142,500W | 6,4 |
| 10 | 4 | 2 AUG 1930 | 57,000S | 135,000W | 6,5 |
| 10 | 4 | 6 JUN 1934 | 56,000S | 140,000W | 6,2 |
| 10 | 5 | 15 DEC 1947 | 59,500S | 160,000W | 7,2 |
| 10 | 6 | 1 JUL 1965 | 63,000S | 163,600W | 6,0 |
| 10 | 6 | 10 APR 1967 | 63,381S | 167,467W | 6,2 |

| | | | | | |
|---|---|---|---|---|---|
| 11 | 1 | 19 SEP 1949 | 54,000S | 2,000W | 6,2 |
| 11 | 1 | 2 JUN 1942 | 54,500S | 4,000W | 6,2 |
| 11 | 2 | 8 JUN 1950 | 47,000S | 15,000W | 7,1 |
| 11 | 2 | 8 AUG 1969 | 47,727S | 15,782W | 6,0 |
| 11 | 3 | 22 AUG 1949 | 36,000S | 18,000W | 6,0 |
| 11 | 3 | 30 SEP 1946 | 37,500S | 17,000W | 6,5 |
| 11 | 3 | 18 JAN 1933 | 37,000S | 18,000W | 6,2 |
| 11 | 3 | 29 NOV 1961 | 37,000S | 18,600W | 6,2 |
| 11 | 4 | 20 AUG 1960 | 35,700S | 15,400W | 6,1 |
| 11 | 4 | 2 AUG 1939 | 36,000S | 16,000W | 6,5 |
| 11 | 4 | 16 JUN 1968 | 36,175S | 15,860W | 6,1 |
| 11 | 5 | 3 APR 1928 | 11,500S | 14,500W | 6,2 |
| 11 | 5 | 20 JUN 1943 | 11,500S | 14,000W | 6,0 |
| 11 | 5 | 29 NOV 1970 | 11,601S | 14,087W | 6,0 |
| 11 | 6 | 7 JUN 1961 | 5,400S | 11,600W | 6,2 |
| 11 | 6 | 30 APR 1932 | 5,000S | 11,500W | 6,0 |
| 11 | 7 | 11 APR 1946 | 1,000S | 14,500W | 7,2 |
| 11 | 7 | 13 APR 1942 | 1,000S | 16,000W | 6,5 |
| 11 | 7 | 19 MAY 1933 | 1,500S | 15,000W | 6,5 |
| 11 | 7 | 19 OCT 1966 | 1,500S | 15,400W | 6,3 |
| 11 | 7 | 20 JUL 1932 | 1,500S | 13,500W | 6,5 |
| 11 | 7 | 6 JUN 1929 | 1,000S | 14,500W | 6,5 |
| 11 | 7 | 3 AUG 1928 | 2,000S | 14,000W | 6,0 |
| 11 | 7 | 4 JUL 1920 | 2,000S | 14,000W | 6,0 |
| 11 | 8 | 6 AUG 1954 | 1,000S | 23,500W | 6,2 |
| 11 | 8 | 7 JUN 1959 | 0,100S | 17,600W | 6,1 |
| 11 | 8 | 19 FEB 1953 | 0,000S | 18,100W | 6,5 |
| 11 | 8 | 16 AUG 1965 | 0,500S | 19,900W | 6,4 |
| 11 | 8 | 15 NOV 1965 | 0,300S | 18,600W | 6,4 |
| 11 | 8 | 4 SEP 1959 | 1,040S | 23,850W | 6,1 |
| 11 | 8 | 3 SEP 1958 | 0,000N | 18,000W | 6,3 |
| 11 | 8 | 30 APR 1954 | 0,000N | 18,500W | 6,0 |
| 11 | 8 | 4 OCT 1949 | 1,000S | 21,000W | 6,2 |
| 11 | 8 | 21 JUL 1941 | 0,250S | 19,500W | 6,0 |
| 11 | 8 | 28 AUG 1973 | 0,199S | 18,027W | 6,8 |
| 11 | 8 | 5 AUG 1971 | 0,853S | 22,130W | 7,0 |
| 11 | 8 | 24 JAN 1941 | 0,500N | 20,000W | 6,0 |
| 11 | 8 | 30 OCT 1940 | 1,500S | 20,000W | 6,2 |
| 11 | 8 | 27 APR 1940 | 1,000N | 19,500W | 6,7 |
| 11 | 8 | 23 APR 1939 | 0,500N | 17,500W | 6,2 |
| 11 | 8 | 2 FEB 1929 | 1,500S | 21,000W | 7,1 |
| 11 | 8 | 12 MAY 1928 | 1,000N | 19,000W | 6,0 |
| 11 | 8 | 18 SEP 1928 | 0,000N | 20,000W | 6,5 |
| 11 | 8 | 5 DEC 1920 | 0,000N | 17,000W | 6,2 |

| | | | | | |
|---|---|---|---|---|---|
| 11 | 9 | 16 NOV 1959 | Ø,89ØN | 26,35ØW | 6,3 |
| 11 | 9 | 9 MAR 1954 | Ø,8ØØN | 29,9ØØW | 6,3 |
| 11 | 9 | 18 JUL 1951 | 1,ØØØN | 27,ØØØW | 6,9 |
| 11 | 9 | 28 DEC 1937 | 1,ØØØN | 29,ØØØW | 6,5 |
| 11 | 9 | 11 OCT 1973 | Ø,636N | 29,514W | 6,3 |
| 11 | 9 | 11 APR 1972 | Ø,967N | 28,286W | 6,4 |
| 11 | 9 | 6 OCT 1937 | 1,5ØØN | 29,ØØØW | 6,2 |
| 11 | 9 | 19 JAN 1935 | 1,ØØØN | 28,ØØØW | 6,7 |
| 11 | 9 | 19 JAN 1935 | 1,ØØØN | 28,ØØØW | 6,2 |
| 11 | 9 | 6 OCT 1934 | 1,ØØØN | 27,ØØØW | 6,3 |
| 11 | 9 | 1 SEP 1934 | Ø,5ØØN | 25,5ØØW | 6,7 |
| 11 | 9 | 22 MAY 1934 | 1,25ØN | 3Ø,25ØW | 6,5 |
| 11 | 9 | 12 OCT 1924 | Ø,5ØØS | 29,ØØØW | 6,5 |
| 11 | 9 | 26 SEP 1923 | 1,5ØØN | 29,5ØØW | 6,Ø |
| 11 | 9 | 8 AUG 1923 | Ø,5ØØN | 3Ø,ØØØW | 6,2 |
| 11 | 9 | 12 NOV 1920 | 1,ØØØN | 28,ØØØW | 6,5 |
| | | | | | |
| 11 | 1Ø | 17 NOV 1963 | 7,6ØØN | 37,4ØØW | 6,6 |
| 11 | 1Ø | 3 AUG 1963 | 7,7ØØN | 35,8ØØW | 6,9 |
| 11 | 1Ø | 1 JUN 1945 | 7,5ØØN | 34,5ØØW | 6,Ø |
| 11 | 1Ø | 28 NOV 1942 | 7,5ØØN | 36,ØØØW | 7,1 |
| 11 | 1Ø | 21 MAR 1941 | 7,ØØØN | 35,ØØØW | 6,5 |
| 11 | 1Ø | 5 NOV 1939 | 7,ØØØN | 34,ØØØW | 6,Ø |
| 11 | 1Ø | 22 AUG 1937 | 7,ØØØN | 36,ØØØW | 6,Ø |
| 11 | 1Ø | 23 JUL 1934 | 7,25ØN | 34,5ØØW | 6,Ø |
| 11 | 1Ø | 31 MAY 1932 | 7,ØØØN | 38,ØØØW | 6,Ø |
| 11 | 1Ø | 27 JAN 1929 | 8,ØØØN | 37,ØØØW | 6,5 |
| 11 | 1Ø | 2Ø MAY 1918 | 7,5ØØN | 36,ØØØW | 7,4 |
| | | | | | |
| 11 | 11 | 25 SEP 1958 | 8,Ø6ØN | 39,29ØW | 6,7 |
| 11 | 11 | 24 APR 1947 | 8,5ØØN | 39,ØØØW | 7,Ø |
| | | | | | |
| 11 | 12 | 17 MAR 1962 | 1Ø,9ØØN | 43,2ØØW | 7,Ø |
| 11 | 12 | 26 JUL 1954 | 11,9ØØN | 43,8ØØW | 6,3 |
| 11 | 12 | 22 FEB 1929 | 11,ØØØN | 42,ØØØW | 7,2 |
| 11 | 12 | 3 SEP 1927 | 11,ØØØN | 44,ØØØW | 6,9 |
| 11 | 12 | 13 OCT 1925 | 11,ØØØN | 42,ØØØW | 7,5 |
| | | | | | |
| 11 | 13 | 22 JUN 1936 | 13,5ØØN | 45,ØØØW | 6,Ø |
| 11 | 13 | 5 JUL 1925 | 13,5ØØN | 42,5ØØW | 6,Ø |
| | | | | | |
| 11 | 14 | 4 MAR 194Ø | 15,25ØN | 45,ØØØW | 6,Ø |
| 11 | 14 | 24 SEP 1969 | 15,237N | 45,776W | 6,4 |
| 11 | 14 | 28 FEB 193Ø | 15,ØØØN | 46,ØØØW | 6,Ø |
| 11 | 14 | 6 JUL 1929 | 14,5ØØN | 46,ØØØW | 6,5 |

| | | | | | |
|---|---|---|---|---|---|
| 12 | 1 | 14 DEC 1964 | 54,900S | 2,400W | 6,2 |
| 12 | 1 | 2 JAN 1960 | 56,000S | 2,000W | 6,1 |
| 12 | 1 | 3 JAN 1971 | 55,503S | 2,578W | 7,1 |
| 12 | 1 | 22 NOV 1928 | 56,500S | 3,000W | 6,9 |
| 12 | 2 | 2 OCT 1958 | 58,000S | 9,500W | 6,0 |
| 12 | 2 | 2 JUN 1963 | 58,300S | 15,300W | 6,3 |
| 12 | 2 | 7 MAR 1925 | 58,000S | 7,000W | 6,5 |
| 12 | 2 | 16 FEB 1925 | 58,000S | 7,000W | 6,7 |
| 12 | 2 | 23 FEB 1932 | 60,000S | 12,500W | 6,9 |
| 12 | 2 | 7 APR 1973 | 58,302S | 13,394W | 6,7 |
| 12 | 2 | 18 MAR 1933 | 59,000S | 15,000W | 6,5 |
| 12 | 2 | 8 SEP 1955 | 58,700S | 19,600W | 6,5 |
| 12 | 3 | 1 OCT 1969 | 60,846S | 19,723W | 6,0 |
| 13 | 1 | 10 NOV 1942 | 49,500S | 32,000E | 7,9 |
| 14 | 1 | 20 JUL 1942 | 35,000S | 99,000W | 6,3 |
| 14 | 1 | 9 APR 1934 | 35,000S | 99,000W | 6,5 |
| 14 | 1 | 12 JUN 1960 | 36,000S | 98,000W | 6,2 |
| 14 | 1 | 23 MAR 1937 | 36,500S | 98,000W | 6,5 |
| 14 | 1 | 22 SEP 1942 | 37,000S | 98,000W | 6,2 |
| 14 | 1 | 23 MAR 1932 | 37,000S | 99,000W | 6,0 |
| 14 | 2 | 9 NOV 1937 | 36,500S | 97,000W | 6,0 |
| 14 | 2 | 30 JUL 1954 | 36,500S | 97,200W | 6,5 |
| 14 | 3 | 11 OCT 1937 | 42,000S | 91,000W | 6,0 |
| 14 | 3 | 14 AUG 1976 | 40,000S | 88,000W | 6,0 |

APPENDIX 2

The following six plots are the geometric mean of the amplitude spectra for each of the six events analyzed in this study. No correction for attenuation has been applied to the spectra.

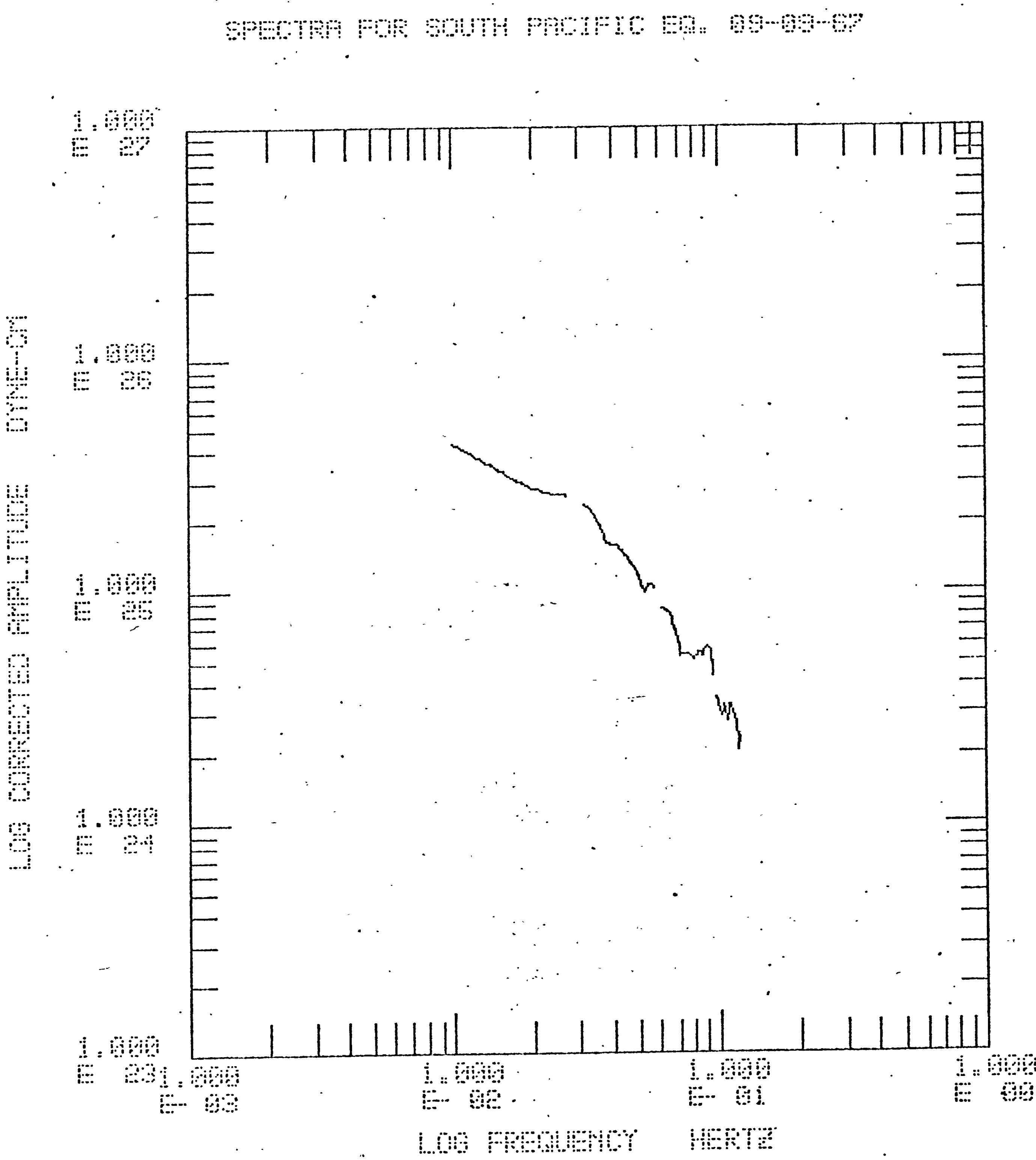
SPECTRA FOR SOUTH PACIFIC EQ. 09-09-67
1.000 E 27
1.000 E 26
1.000 E 25
1.000 E 24
1.000 E 23
LOG CORRECTED AMPLITUDE DYNE-CM
1.000 E- 03
1.000 E- 02
1.000 E- 01
1.000 E 00
LOG FREQUENCY HERTZ

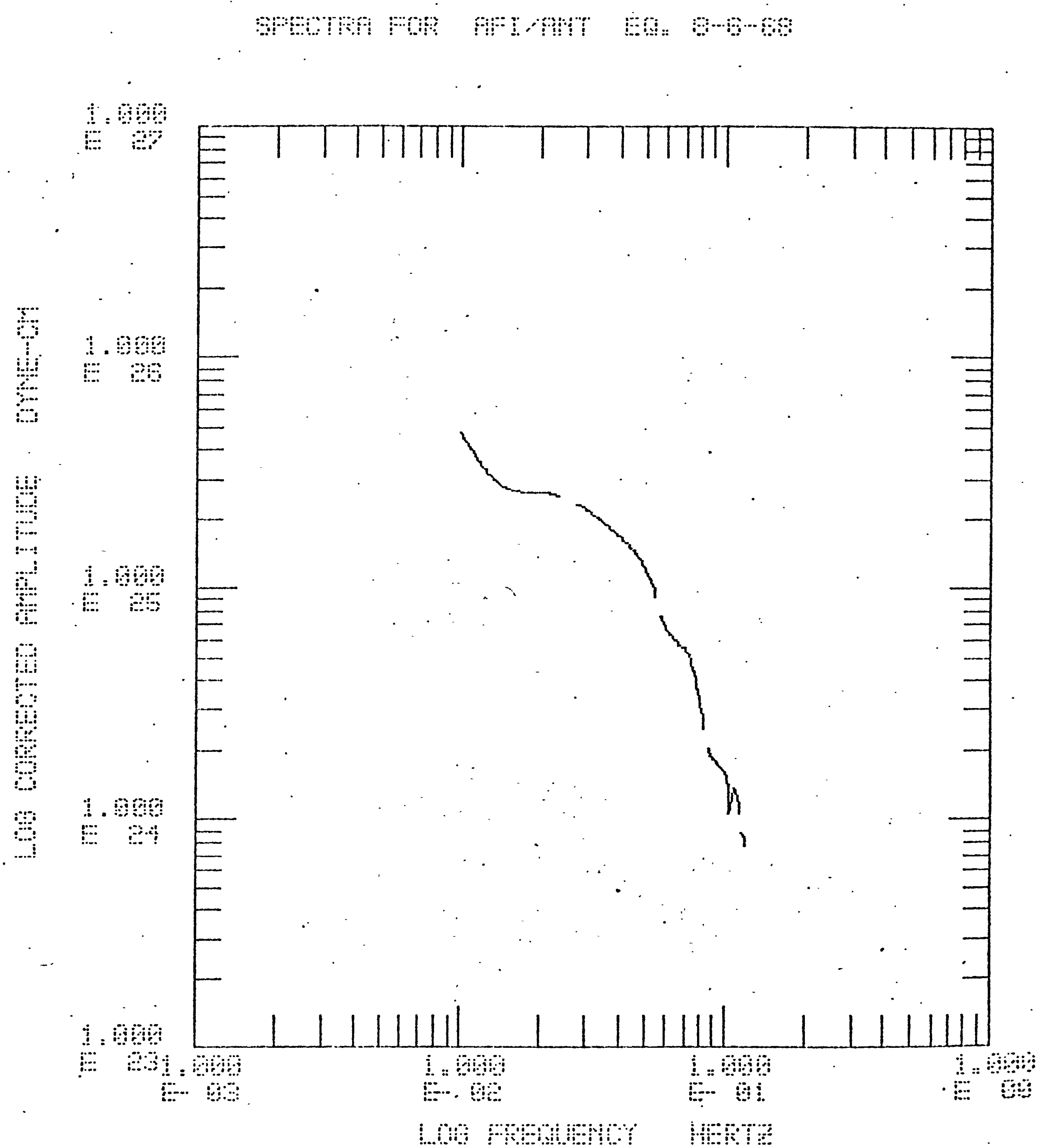
SPECTRA FOR AFI/ANT EQ. 8-6-68
LOG CORRECTED AMPLITUDE DYNE-CM
1.000 E 27
1.000 E 26
1.000 E 25
1.000 E 24
1.000 E 23
1.000 E- 03
1.000 E- 02
1.000 E- 01
1.000 E 00
LOG FREQUENCY HERTZ

SPECTRA FOR EQ 18-8-69 IN SOUTH PACIFIC

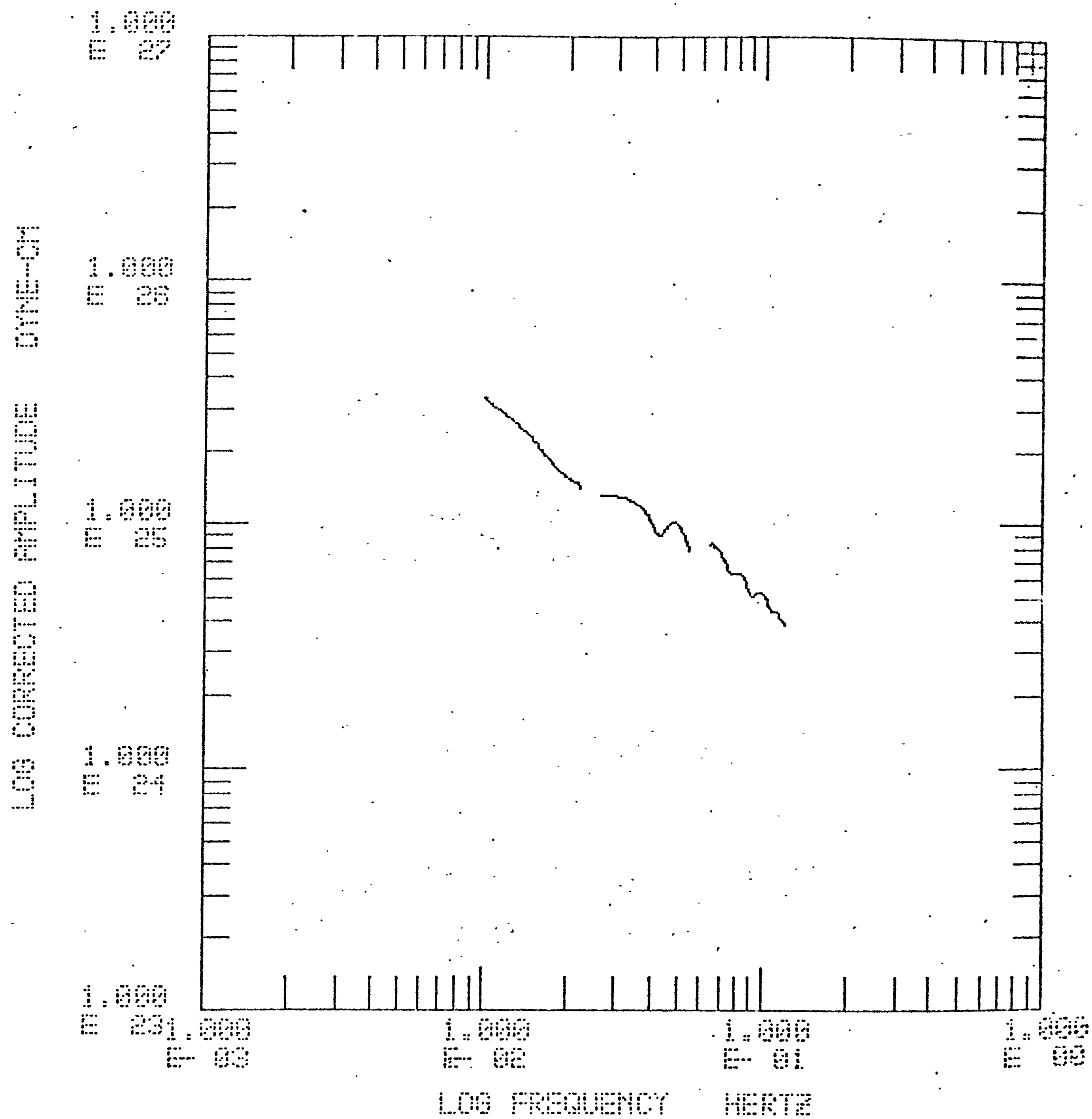

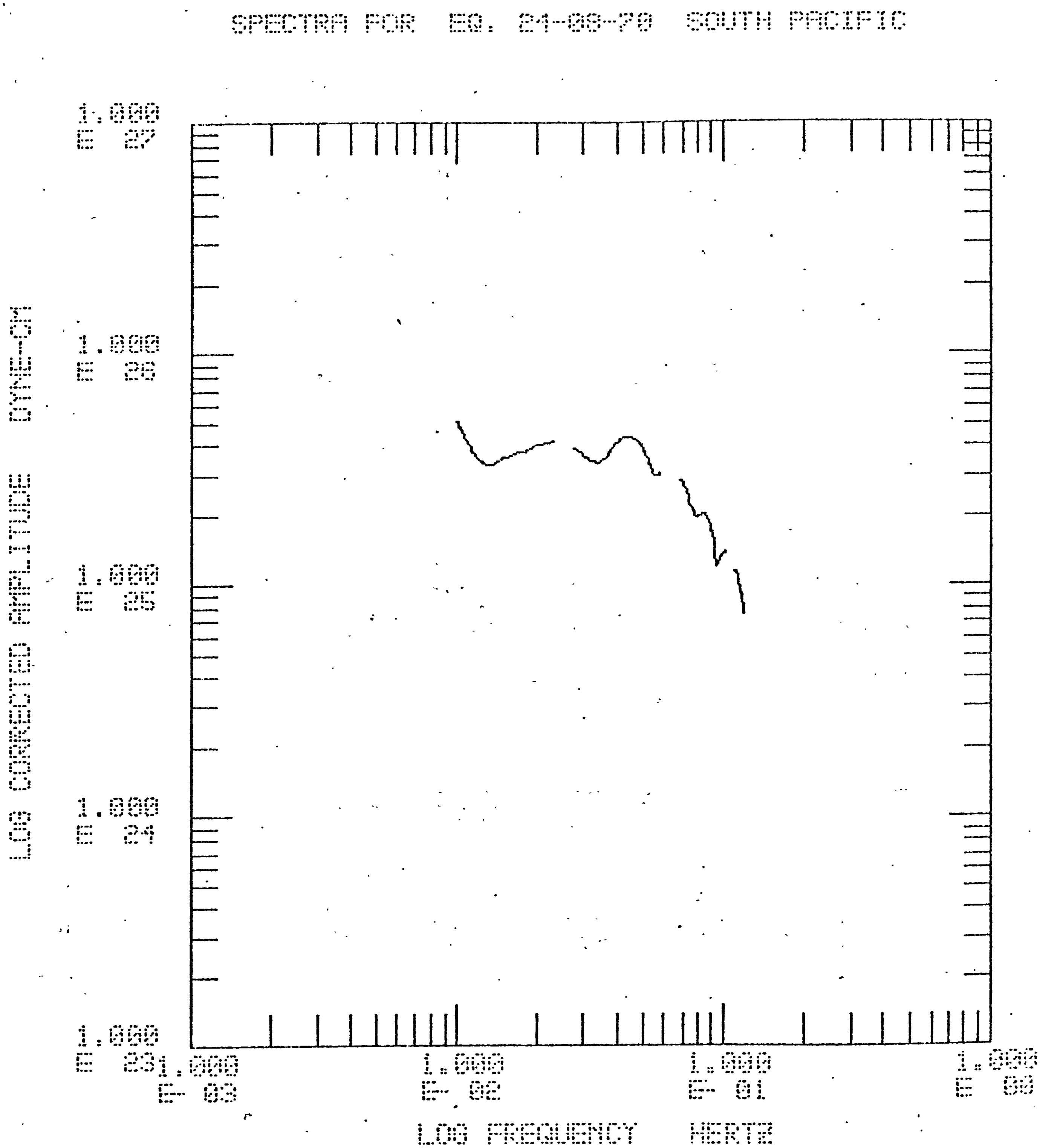
SPECTRA FOR EQ. 24-08-70 SOUTH PACIFIC
LOG CORRECTED AMPLITUDE DYNE-CM
1.000 E 27
1.000 E 26
1.000 E 25
1.000 E 24
1.000 E 23
1.000 E- 03
1.000 E- 02
1.000 E- 01
1.000 E 00
LOG FREQUENCY HERTZ

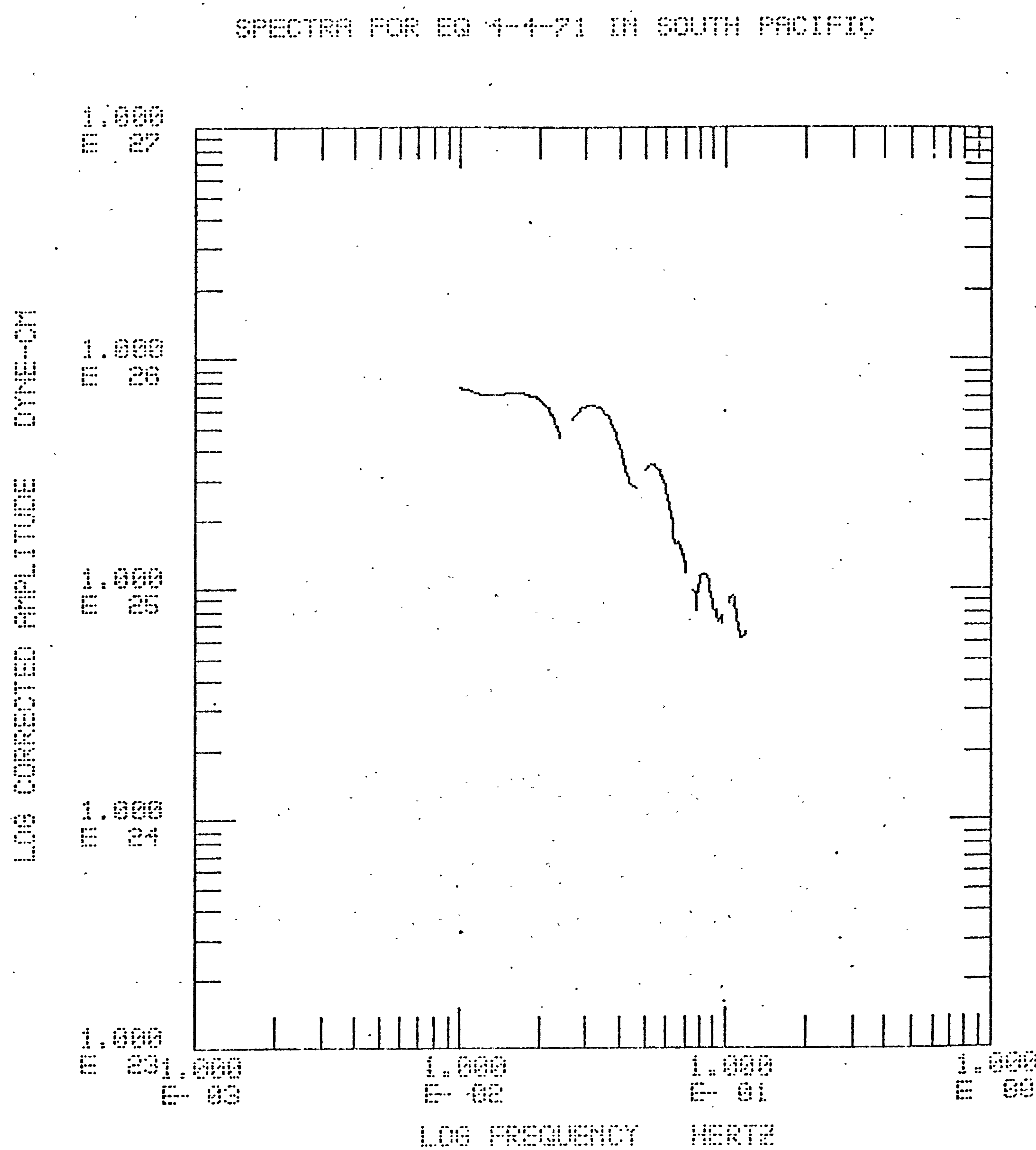
SPECTRA FOR EQ 4-4-71 IN SOUTH PACIFIC
LOG CORRECTED AMPLITUDE DYNE-CM
1.000 E 27
1.000 E 26
1.000 E 25
1.000 E 24
1.000 E 23
1.000 E-03
1.000 E-02
1.000 E-01
1.000 E 00
LOG FREQUENCY HERTZ

SPECTRA FOR AFI/ANT EQ. 8-1-74